Research Square

Preprints are preliminary reports that have not undergone peer review.
They should not be considered conclusive, used to inform clinical practice,
or referenced by the media as validated information.

Deciphering the Molecular Mechanisms Underlying Avocado Dieback Disease Caused by *Neofusicoccum luteum*

Beatriz Santos Casanova
Andalusian Institute of Agricultural and Fisheries Research and Trainingm
Enrique López Gomez
Instituto de Hortofruticultura Subtropical y Mediterránea "La Mayora"
Ana Moreno Pérez
Andalusian Institute of Agricultural and Fisheries Research and Trainingm
Lucia Guirado Manzano
Universidad de Málaga
David Ferrer
Instituto de Hortofruticultura Subtropical y Mediterránea "La Mayora"
Francisco M. Cazorla
Universidad de Málaga
Eva Arrebola Díez
Universidad de Málaga
Noe Fernandez Pozo
Instituto de Hortofruticultura Subtropical y Mediterránea "La Mayora"
Clara Pliego
mclara.pliego@juntadeandalucia.es

Andalusian Institute of Agricultural and Fisheries Research and Trainingm

Research Article

Keywords: Neofusicoccum luteum, avocado dieback, Botryosphaeriaceae, comparative genomics, transcriptomics, effector proteins, virulence factors

Posted Date: July 9th, 2026

DOI: https://doi.org/10.21203/rs.3.rs-10127271/v1

License: This work is licensed under a Creative Commons Attribution 4.0 International License. Read Full License

Additional Declarations: No competing interests reported.

Abstract

Background

Neofusicoccum luteum is a major causal agent of avocado dieback disease, causing significant economic losses in major producing regions including California, Italy, and Spain. Despite its global importance, the molecular mechanisms underlying *N. luteum* pathogenicity and tissue-specific infection strategies remain poorly understood. To address this knowledge gap, we sequenced and assembled the complete genome of the virulent *N. luteum* strain UMAF A1963 and performed transcriptomic analysis of the infection of avocado branches and fruits compared to in vitro growth on potato dextrose agar.

Results

The high-quality genome assembly (40.82 Mb, N50 = 2.10 Mb) achieved 95% completeness based on Benchmarking Universal Single-Copy Orthologs (BUSCO) analysis and revealed 664 carbohydrate-active enzyme genes (CAZyme), indicating robust plant cell wall degradation capacity. Comparative genomic analysis with related Botryosphaeriaceae species showed extensive conservation, with 7,300 of 10,842 gene clusters (67%) forming a shared core genome, while species-specific clusters reflect lineage-specific adaptations. RNA-seq analysis revealed extensive transcriptional reprogramming during infection, with 2,875 and 2,419 differentially expressed genes identified in branch and fruit infections, respectively, compared to in vitro culture. Functional enrichment analysis revealed tissue-specific strategies: branch infection was characterized by protein refolding, cellulose metabolism, and siderophore processes, while fruit infection showed enhanced carbohydrate transport, glycosphingolipid metabolism, and mitochondrial functions. Among the 235 candidate virulence factors identified, cell wall-degrading enzymes (CWDEs), proteases, and fungal toxins were the most prevalent functions, followed by others such as hormone metabolism, transport proteins, stress response factors, detoxification enzymes, and transcriptional regulators. Genome-wide effector prediction identified 2,745 candidates, with 38 high-confidence effectors showing homology to characterized pathogenicity factors and exhibiting both apoplastic and cytoplasmic targeting patterns. Notably, a putative pectate lyase (*NelutCtg15g0740.1*) achieved exceptional upregulation (FC = 2,129.81 in branches; FC = 19,186.08 in fruits) and was predicted as a dual-localization effector with 54% cytoplasmic and 76% apoplastic probabilities.

Conclusions

This study provides the first comprehensive molecular characterization of *N. luteum* pathogenicity, revealing sophisticated tissue-specific virulence strategies mediated by coordinated expression of cell wall-degrading enzymes, transport systems, detoxification mechanisms, hormone metabolism and effector proteins. The genomic resources and mechanistic insights generated establish a foundation for developing targeted management strategies against avocado dieback disease and advance our understanding of Botryosphaeriaceae pathogenesis.

Background

Trunk diseases caused by fungi belonging to the Botryosphaeriaceae family are a significant phytopathological concern, affecting various woody plants including crops, conifers and ornamental species. They are of particular concern in temperate and subtropical regions, where they affect species such as grapevines, olives, citrus fruits and stone fruits [1–5]. Avocados are among the crops most severely impacted by this disease worldwide [6, 7]. This crop holds an important position in global agriculture and economic development with Spain being the largest avocado producer in Europe, leveraging its proximity to European markets, with production mainly concentrated in Andalusia and along the southern coast.

The Botryosphaeriaceae family comprises numerous morphologically similar species of ascomycete fungi. These facultative aerial parasites and saprophytes are also found in nature as endophytes. The species most frequently associated with damage in avocado trees belong to the genera *Botryosphaeria*, *Dothiorella*, *Diplodia*, *Lasiodiplodia* and *Neofusicoccum*. Previous studies conducted in Spain have revealed *Neofusicoccum* and *Lasiodiplodia* to be the main causal agents of avocado dieback disease [8, 9]. Specifically, most of the analysed isolates belonged to different *Neofusicoccum* species, with *N. luteum* being one of the most abundant.

N. luteum, as other species of the Botryosphaeriaceae family, has the capacity to produce two distinct types of fruiting bodies: perithecia (sexual) that release ascospores and pycnidia (asexual) that release conidia. The sexual stage is rarely observed, while the asexual stage is more common. The pycnidia are found on the bark, branches, leaves, and fruits of the infected plant (whether living or dead). In moist conditions, the conidia (asexual spores) are released and dispersed, primarily by means of rain splashes and wind or by contact between affected plants [10, 11]. The precise mechanism by which penetration into the host occurs remains to be elucidated; however, it is hypothesized that the conidia enter the host through various openings, either through wounds or through stomata and lenticels. Direct penetration of this fungus could also occur through appressorium-like structures. Once inside the host, this fungus can become endophytic, remaining dormant inside the plant without causing symptoms until conditions become favorable for infection. In circumstances where the plant is experiencing stress (for example, as a result of drought, physical damage or nutrient deprivation), the latent fungus present within the plant may begin to act as a pathogen, thus causing symptoms of the disease [12–14].

Effective control of *N. luteum* is especially challenging due to its endophytic nature and activation under abiotic stress conditions, which makes early detection and management difficult [13]. Despite the successful outcomes observed when using fungicides on other crops, there are no fungicides that can be used to control the disease caused by this fungus in avocados. Furthermore, there are no effective biocontrol agents or resistant cultivars available [14]. Consequently, management of this disease is currently limited to cultural practices aimed at preventing its transmission and spread. A number of practices have been identified as effective in managing these issues. These include pruning and harvesting in conditions of low humidity, as well as providing adequate

irrigation and fertilization. It is also important to avoid plant stress as much as possible (nutritional or water-related), as well as reducing damage caused by other pests and diseases [15, 16].

To improve future disease resistance, the systematic analysis of pathogenic fungi's genomes and transcriptomics studies of plant pathogenic fungi/host interactions is a top priority. To date, few species within the Botryosphaeriaceae family have been sequenced *(B. dothidea*, *L. theobromae* and *N. parvum*) [17–19], improving the understanding of their pathogenicity mechanisms [14]. Belair et al. [20] performed a comparative analysis of 41 genomes representing six Botryosphaeriaceae genera to gain insight into genetic features associated with pathogenicity and virulence. Results showed that these Botryosphaeriaceae genomes possess a high degree of diversity in terms of carbohydrate-active enzymes (CAZymes; 128 families) and peptidases (45 families). The highest number of genes encoding CAZymes involved in the degradation of plant cell wall components were found in *Botryosphaeria*, *Neofusicoccum*, and *Lasiodiplodia*. With regard to secondary metabolite gene clusters, the findings were consistent across the family, with exceptions in *Diplodia*, where the number was notably lower. Chromatography mass spectrometry studies performed on liquid cultures of different *Neofusicoccum* species have identified a number of secondary metabolites, including botryoisocoumarin A, botryosphaerones, cyclobotryoxide and isosclerone [21]. These compounds show structural variability and bioactivities, which might be associated with their role in fungal pathogenicity and virulence.

Complementary transcriptomic studies have further clarified pathogenic mechanisms within the Botryosphaeriaceae. In the *Neofusicoccum parvum*–walnut pathosystem, comparative transcriptome analysis highlighted the pivotal role of ATP-binding cassette (ABC) transporters in virulence, with the ABC1 transporter specifically implicated in enabling the fungus to tolerate hostile host conditions during infection [22]. Additionally, the involvement of secreted enzymes associated with host tissue colonization has been experimentally confirmed, underscoring the importance of degradative processes in disease development [23].

More recently, an integrated transcriptomic and metabolomic investigation of the *N. parvum*–peach gummosis interaction revealed that the pathogen modulates genes related to plant cell wall degradation and UDP-sugar metabolism to facilitate invasion of peach shoot tissues and induce gum secretion [24]. These findings support a model in which Botryosphaeriaceae pathogens actively reprogram host metabolic pathways to promote colonization and symptom expression.

Genomic resources are also essential for accurate species identification within this taxonomically complex family [4]. Molecular diagnostics have been substantially improved through the development of robust genetic markers and optimized primer sets targeting lineage-specific sequences. Multilocus sequence analysis using regions such as Internal transcribed spacer region of ribosomal (ITS), β-tubulin (TUB), translation elongation factor 1-a (EF1-a) and RNA polymerase II second largest subunit (rpb2) has proven particularly effective for resolving species boundaries within Botryosphaeriaceae [25–28]. More recently, highly transferable microsatellite or simple sequence repeat (SSR) markers have been developed for species of *Lasiodiplodia* and *Neofusicoccum*, enabling detailed population genetic studies and facilitating the detection and discrimination of a broad range of taxa within these genera [29].

Despite these advances, functional genomics in the Botryosphaeriaceae family remains an emerging field, and to date, no research has addressed the Botryosphaeriaceae–avocado pathosystem. To address this gap, we sequenced and assembled the complete 40 Mb genome of *N. luteum* strain UMAF A1963, a virulent isolate from Spanish avocado orchards. We then performed comparative RNA-seq analysis of the fungus during colonization of 'Hass' avocado branches and fruit relative to its in vitro growth on PDA medium. This dual-tissue approach aimed to identify tissue-specific virulence determinants providing a foundation for developing targeted management strategies against avocado dieback disease.

Material and methods

Plant material, fungal isolate and inoculation

Four-year-old 'Dusa' clones grafted with 'Hass' and described as susceptible to *N. luteum* were provided by Brokaw Nursery (Brokaw España S.L.). and placed in a semi-controlled greenhouse with a temperature of ~ 20°C and relative humidity of ~ 60%. The virulent UMAF A1963 fungal strain, which was isolated in Axarquía (Málaga, Spain), was cultured on potato dextrose agar (PDA) (Difco Laboratories, Detroit, USA) at 25°C for this study.

To analyse the genome of *N. luteum*, the isolate was cultured on PDA covered with a perforated layer of cellophane and incubated for four days at 25°C.

To analyse the *N. luteum* transcriptome during growth on a nutrient-rich medium, 2 mm plugs of the isolate was cultured on PDA plates covered with a perforated layer of cellophane and incubated at 25°C for five days.

For RNA-Seq analysis during fruit and branch infection, avocado fruits (cv. 'Hass') and detached Hass stems (10 cm in length) were surface-disinfected by immersion for 5 min in a mixture of ethanol, commercial bleach, and distilled water (1:2:7, v/v/v), followed by two successive rinses in sterile distilled water for 5 min each. Fruits and stems were maintained under humidity-saturated conditions and covered with a perforated layer of cellophane prior to inoculation. Inoculation was performed as previously described by Crespo et al. [31], and samples were incubated at 25°C for five days.

DNA isolation and sequencing

Genomic DNA was extracted following the CTAB-based protocol of Healey et al. [31] with minor modifications. Briefly, five-day-old mycelium grown on potato dextrose agar (PDA) was harvested, freeze-dried, and ground to a fine powder using a mortar and pestle. Approximately 100 mg of powdered tissue was incubated at 65°C for 30 min in 600 µL of preheated lysis buffer (2% CTAB, 100 mM Tris-HCl pH 8.0, 1.4 M NaCl, 1% PVP-40, 20 mM EDTA) supplemented with 3 µL β-mercaptoethanol.

An equal volume of cold chloroform:isoamyl alcohol (24:1, v/v) was added, mixed thoroughly, and centrifuged at 13,500 × g for 10 min at 4°C. The aqueous phase was transferred to a new 2-mL microcentrifuge tube, and the extraction step was repeated twice. DNA was precipitated by adding 0.7 volumes of cold isopropanol and incubating at − 20°C for 30 min, followed by centrifugation at 21,900 × g for 15 min at 4°C. The resulting pellet was washed twice with 70% ethanol, air-dried, and resuspended in 100 µL DNase-free water.

RNA was removed by treatment with RNase A (Qiagen). DNA concentration and purity were determined using a NanoDrop® ND-1000 (Nanodrop Technologies, Inc., Wilmington, NC, USA) and Qubit fluorometer, and integrity was assessed by agarose gel electrophoresis. DNA samples were submitted to Novogene Sequencing-Europe (Cambridge, U.K.) for library preparation and sequencing. A total of 1.0 µg genomic DNA per sample was used as input. Sequencing libraries were prepared using the NEBNext® DNA Library Prep Kit according to the manufacturer's instructions, with index sequences added to each sample. Genomic DNA was randomly fragmented to an average size of ~ 350 bp by mechanical shearing, followed by end repair, A-tailing, and ligation of NEBNext adapters for Illumina sequencing. Adapter-ligated fragments were PCR-enriched using P5 and indexed P7 primers. PCR products were purified using the AMPure XP system, and library size distribution was assessed with an Agilent 2100 Bioanalyzer. Library concentration was determined by quantitative PCR.

Libraries from three biological replicates of *N. luteum* strain UMAF A1963 cultured on PDA were sequenced using Illumina NovaSeq PE150 at the Beijing Novogene Bioinformatics Technology Co., Ltd.

Genome assembly

Raw reads were filtered to remove low-quality reads, reads containing ambiguous bases, and adapter-contaminated sequences, generating clean data for downstream analysis. After clean data was obtained, the assembly was first performed using SOAPdenovo (version 2.04) [32], SPAdes [33], and ABySS [34] assembling software, and finally using CISA [35] software for integration. The produced genome was annotated with GeneMark [36]. The completeness of the gene set was assessed using Benchmarking Universal Single-Copy Orthologs (BUSCO) v5.8.2 [37] with the fungi_odb10 and dothideomycetes_odb10 lineage datasets.

Data integration into AvoBase

N. luteum genomic data and its annotations were integrated into AvoBase following the instructions of the EasyGDB [38] manual (https://github.com/noefp/easy_gdb). The code for the *N. luteum* custom page in AvoBase is available in the GitHub AvoBase repository (https://github.com/noefp/avocadobase).

RNA isolation and sequencing

For RNA extraction, cellophane discs covered with actively growing mycelium were collected from three biological replicates per condition, each biological replicate consisting of a mixture of three technical replicates, and immediately frozen in liquid nitrogen. Samples were ground to a fine powder using a pre-chilled mortar and pestle. Approximately 1 g of frozen powder was transferred to a 2 mL microcentrifuge tube and resuspended in 1 mL of denaturation solution containing 4 M guanidine thiocyanate, 25 mM sodium citrate, and 0.5% sarcosyl (Fluka, Switzerland), mixed 1:1 with saturated phenol (pH 4.3) and supplemented with 7 µL β-mercaptoethanol.

Subsequently, 100 µL chloroform was added, samples were vortexed, incubated for 3 min at room temperature, and centrifuged at 12,000 x g for 10 min at 4°C. The aqueous phase was then used for RNA purification with the NucleoSpin® RNA Plant kit (Macherey-Nagel, Germany) according to the manufacturer's instructions.

DNAase I (DNase I, Thermo, USA) treatment was carried out twice, during and after the extraction process. RNA quantity and quality were determined based on absorbance ratios at 260 nm/280 nm and 260 nm/230 nm using a NanoDrop® ND-1000 (Nanodrop Technologies, Inc., Montchanin, USA) spectrophotometer. RNA integrity was confirmed by the appearance of ribosomal RNA bands and lack of degradation products after separation on a 2% agarose gel and Red Safe staining.

The samples were submitted to Novogene Sequencing-Europe (U.K., Cambridge Sequencing Center) for sequencing. Two µg of each sample were used for RNA library preparation. Messenger RNA was purified from total RNA using poly-T oligo-attached magnetic beads. After fragmentation, the first strand cDNA was synthesized using random hexamer primers, followed by the second strand cDNA synthesis using either dUTP for directional library or dTTP for non-directional library. For the non-directional library, it was ready after end repair, A-tailing, adapter ligation, size selection, amplification, and purification. The library was checked with Qubit and real-time PCR for quantification and bioanalyzer for size distribution detection. Each library was sequenced aiming for 30 million reads per sample (9G of raw data PE 150), using the Illumina NovaSeq 6000 platform. RNA-Seq libraries were prepared with three biological replicates per condition (branch and PDA). For infected fruit samples, however, one replicate failed, and only two libraries were successfully sequenced.

Transcriptome data processing and analysis

Raw sequencing reads were evaluated with FastQC v0.11.9 (https://www.bioinformatics.babraham.ac.uk/projects/fastqc) and MultiQC v1.13a [39]. Quality filtering and adapter trimming were performed using Trimmomatic v0.39 [40], with parameters ILLUMINACLIP:TruSeq3-PE.fa:2:30:10 LEADING:3 TRAILING:3 SLIDINGWINDOW:4:15 MINLEN:36. The processed reads were mapped to the *N. luteum* assembly produced in this work using HISAT2 v2.2.1 [41], and the

resulting alignments were converted to sorted BAM files with SAMtools v1.16 [42]. Finally, gene expression was quantified at the coding sequence (CDS) level using featureCounts from the Subread package v2.0.6 [43].

Principal component analysis (PCA) and specific gene identification were conducted using R v.4.4.1. For the PCA analysis, raw gene counts were normalized to Counts per Million (CPM) using the edgeR package [44], and the clustering was performed using the prcomp function from the stats package. Raw gene counts were normalized to Transcripts per Million (TPM) using the convertCounts function from the R package DGEobj.utils, and genes with a minimum expression threshold of TPM ≥ 1 were considered for the Venn diagram of shared and specific transcripts present across the samples.

Gene expression and enrichment analysis were also performed in R. For differential gene expression analysis, DESeq2 v1.46.0 [45] was employed to normalize gene expression data and identify differentially expressed genes (DEGs). Orthologs between *Neofusicoccum luteum* and *Aspergillus nidulans* were identified using Diamond BLASTp v2.1.8.162 [46]. Reciprocal best hits were retained, and matches with a bit-score below 45 were filtered out. The *A. nidulans* proteins most similar to the identified DEGs were used for the functional enrichment analysis, which was performed using the OrgDb package for *A. nidulans* FGSC A4, available at the repository https://github.com/lakhanp1/fungal_resources, and a custom script (https://github.com/bullones/FunRichR) based on the clusterProfiler package v.4.14.6 [47].

Results

Genome sequencing and assembly

The assembly of the *N. luteum* genome resulted in an estimated total size of 40.82 Mb. The assembly contained a total of 48 contigs, with an N50 value of 2.10 Mb and a L50 value of 9 sequences. The length of the longest contig was 3.14 Mb, while the shortest contig had a length of 5.49 kb. Genome completeness was evaluated using BUSCO v5.8.2 [37, 48], showing that for the Fungi and Dothideomycetes lineages, approximately 95% of BUSCO genes were found to be complete in the genome, less than 0.2% were duplicated, and only 3.5% were not detected (Fig. 1). Together, these metrics show that the assembled *N. luteum* genome is highly complete and exhibits very low sequence duplication, representing a high-quality assembly for a non-model pathogenic fungus.

To facilitate research of *N. luteum*, comprehensive genomic resources produced in this study have been integrated into AvoBase (https://www.avocado.uma.es/), a web portal dedicated to avocado genomics. This specialized repository provides access to the genome assembly of *N. luteum*, and a suite of analysis tools such as genome browser, BLAST, annotation search, annotation and sequence extraction for a list of genes, and a gene expression atlas for the avocado branch and fruit infection study.

Comparative genomic analysis of N. luteum and related Botryosphaeriaceae species

A comparative analysis of the genome of *N. luteum* was conducted with other members of the *Botryosphaeriaceae* family, including *Neofusicoccum parvum*, *Botryosphaeria dothidea* and *Lasiodiplodia theobromae*.

A study of CAZymes revealed that *N. luteum* possesses a total of 664 CAZyme-related genes, comprising 307 glycoside hydrolases (GHs), 145 auxiliary activities (AAs), 111 glycosyltransferases (GTs), 44 carbohydrate esterases (CEs), 31 carbohydrate-binding modules (CBMs), and 26 polysaccharide lyases (PLs) (Fig. 2).

The CAZyme repertoire of *N. luteum* exhibited a high degree of similarity with that of closely related species within the Botryosphaeriaceae family. A comparable distribution of enzyme classes was observed with *N. parvum*, the most closely related species, which displayed nearly identical numbers across all CAZyme categories. *B. dothidea* and *L. theobromae* exhibited a slightly higher number of CAZymes, particularly within the GH and GT classes. Across all species analysed, GHs represented the most abundant CAZyme class, followed by AAs and GTs, whereas CBMs and PLs were less represented. This conserved distribution suggests a comparable CAZyme composition among members of the Botryosphaeriaceae family. The relative abundance of GHs and AAs is consistent with the presence of enzymes involved in the degradation of plant cell wall components, such as cellulose, hemicellulose, and lignin.

Orthologous gene clustering analysis was performed in order to compare the four analysed species, revealing a total of 10,842 gene clusters distributed across shared and species-specific categories (Fig. 3). A large core genome was identified, comprising 7,300 gene clusters shared by all four species, indicating a high level of conservation among these genomes. Beyond the core genome, the accessory genome encompassed multiple species-specific combination subsets. The largest shared cluster groups were identified among *N. luteum*, *B. dothidea*, and *L. theobromae* (876 clusters), followed by *B. dothidea* and *L. theobromae* (548 clusters), and *N. parvum*, *B. dothidea*, and *L. theobromae* (380 clusters), with additional smaller subsets distributed across remaining species combinations (Fig. 3).

In the case of *N. luteum*, a limited number of 10 species-specific gene clusters were identified, in contrast to *B. dothidea* and *L. theobromae*, which exhibited 194 and 89 unique clusters, respectively, while *N. parvum* showed the lowest number with only 5. It is important to note that *N. luteum* and *N. parvum*, which are closely related, exhibited a similarly low number of species-specific clusters. The low number of *N. luteum* specific clusters, in combination with its high number of shared clusters with other species, reflects a high degree of genomic conservation.

Comparative transcriptome analysis of N. luteum growing on avocado fruits and branches vs PDA medium

RNA-Seq analysis was performed to identify genes expressed by the virulent *N. luteum* strain UMAF A1963 during colonization of susceptible 'Hass' avocado branches (NLB) and fruits (NLF) relative to growth under in vitro conditions on potato dextrose agar (NLPDA) (Fig. 4). To assess data quality and inter-replicate reproducibility prior to differential expression analysis, principal component analysis (PCA) was performed on normalized read counts across all

samples (Fig. 5). PCA of the three sample groups revealed clear separation along the first two principal components, which together accounted for 85% of the total variance (PC1 = 65%, PC2 = 20%). NLB and NLPDA samples were strongly separated along PC1, occupying opposite ends of the axis. NLF samples formed a distinct cluster in the lower region of the plot, clearly separated from both NLB and NLPDA. PCA demonstrated that the transcriptional profiles of the three groups are highly distinct, supporting their use as biologically meaningful comparisons in subsequent differential expression analyses (Fig. 5).

The quantification of the three experimental conditions (NLB, NLF and NLPDA) revealed a total of 10,153 expressed transcripts, of which 9,408 were detected across all three conditions. Shared expression between NLB and NLF, NLF and NLPDA, and NLB and NLPDA was observed for 244, 79, and 92 transcripts, respectively, while 176, 63, and 91 transcripts were exclusively expressed under NLB, NLF, and NLPDA conditions, respectively (Fig. 6a). Differential gene expression analysis across pairwise comparisons revealed distinct transcriptional responses among the two groups (Fig. 6b). A substantially larger number of DEGs was observed in the NLB versus NLPDA comparison (2,875 DEGs), where induced genes were slightly predominant (53.67% induced, 46.33% repressed). Similarly, the NLF versus NLPDA comparison identified 2,419 DEGs, with induced genes representing the majority (56.26% induced, 43.74% repressed).

Genes potentially involved in the pathogenesis of N. luteum

Comparative transcriptomic analysis between infected tissues and in vitro cultures revealed 2,875 differentially expressed genes (DEGs) in the NLB vs. NLPDA comparison and 2,419 DEGs in the NLF vs. NLPDA comparison (fold change (− 2 > fold change (FC) > 2; $P < 0.05$). Among these, 235 transcripts showed significant homology to genes previously implicated in fungal virulence. These candidate virulence factors encompassed diverse functional categories, including cell wall-degrading enzymes (CWDEs), proteases, fungal toxins, hormone related, transport proteins, stress tolerance, detoxification enzymes, and transcriptional factors (Supplementary Table 1).

Sixty-one genes were annotated as CWDEs, representing a major component of the putative virulence arsenal. The majority (57 genes, 93.4%) encoded CAZymes, distributed across five functional classes: AAs (n = 4), CBMs (n = 2), CEs (n = 4), GHs (n = 46), and PLs (n = 1). Four additional transcripts (*NelutCtg26g0570.1*, *NelutCtg12g3820.1*, *NelutCtg01g6850.1*, *and NelutCtg05g3780.1*) were classified as CWDEs but fell outside the CAZyme classification system (Supplementary Table 1). Remarkably, two CAZyme-encoding genes (*NelutCtg15g0740.1* and *NelutCtg20g1770.1*) ranked among the top 10 most highly upregulated transcripts during infection in both tissue types. In branch tissues, these genes exhibited fold changes of 2,129.81 and 62.48, respectively, while in fruit tissues, expression levels reached 19,186.09 and 232.63-fold increases compared to axenic culture conditions (Table 1).

Nineteen genes encoding putative proteases were identified, with the majority showing consistent upregulation during infection of both branch and fruit tissues. One notable exception was a putative peptidase S8/S53 subtilisin kexin sedolisin protein (*NelutCtg04g3310.1*), which exhibited modest downregulation during fruit infection (FC = − 1.30) (Table 1).

Tissue-specific expression patterns were observed among protease genes. In branch tissues, a putative peptidase M35 deuterolysin protein (*NelutCtg27g0350.1*) displayed the highest induction level (FC = 399.71), while showing only marginal upregulation in fruit tissues (FC = 1.91). Conversely, a putative metalloprotease (*NelutCtg14g3410.1*) emerged as the most strongly upregulated protease in fruit tissues (FC = 22.68) but exhibited lower expression levels in branch tissues (FC = 6.93), suggesting tissue-specific roles in pathogenesis (Table 1).

Multiple genes associated with toxin biosynthesis exhibited significant upregulation during infection, with several displaying pronounced tissue-specific expression patterns. The most highly induced transcript was a putative sterigmatocystin biosynthesis monooxygenase (*stcW*) (*NelutCtg27g1070.1*), which showed substantially greater expression in branch tissues (FC = 1,972.63) compared to fruit tissues (FC = 608.10) (Supplementary Table 1). A second *stcW* homolog (*NelutCtg22g1170.1*) followed a similar expression pattern, exhibiting strong upregulation in branches (FC = 251.39) relative to fruit (FC = 90.81) (Table 1).

Conversely, some toxin biosynthesis genes displayed preferential expression in fruit tissues. A putative tri7-like toxin biosynthesis protein (*NelutCtg29g0240.1*) was consistently upregulated in both tissues but showed higher expression levels in fruit (FC = 126.92) compared to branches (FC = 54.53). Genes involved in aflatoxin biosynthesis and regulation, including an aflatoxin regulatory protein and nor-1 (aflatoxin biosynthesis ketoreductase) (*NelutCtg32g0150.1*), exhibited moderate but consistent upregulation across both tissue types (Supplementary Table 1).

Thirty-six differentially expressed genes were functionally associated with detoxification processes, underscoring their potential significance in *N. luteum* pathogenicity. The majority of detoxification-related genes were upregulated during infection (32 genes in branches and 29 genes in fruit), with branch infections generally exhibiting higher expression levels than fruit infections (Supplementary Table 1).

The detoxification response was led by a putative pisatin demethylase (*NelutCtg29g0320.1*), which achieved the highest expression levels (FC = 302.32 in branches vs. 205.81 in fruit). This was followed by a short-chain dehydrogenase/reductase (SDR) (*NelutCtg09g0820.1*) showing substantial upregulation (FC = 297.76 in branches vs. 143.48 in fruit) and a putative α/β-hydrolase (*NelutCtg23g0410.1*) displaying pronounced tissue-specific differences (FC = 253.02 in branches vs. 72.64 in fruit) (Table 1). These expression patterns indicate robust activation of xenobiotic detoxification pathways during host colonization.

Additional components of the detoxification machinery included aldo-keto reductases and putative antibiotic biosynthesis monooxygenases, which demonstrated consistently elevated expression across both tissue types, suggesting their fundamental role in overcoming host chemical defenses.

Cytochrome P450 monooxygenases, which serve as key enzymes in both detoxification and secondary metabolism, displayed moderate upregulation during infection. However, tissue-specific variation was observed, with one transcript (*NelutCtg21g0160.1*) showing significant downregulation in fruit tissue (FC = − 14.18). Similarly, genes encoding glyoxalase/bleomycin resistance proteins and alcohol dehydrogenases exhibited contrasting expression patterns between tissues, with repression in fruit but induction in branch tissues (*NelutCtg08g1390.1*, *NelutCtg18g1170.1*, and *NelutCtg21g0190.1*) (Supplementary Table 1).

Additional detoxification enzymes, including catalases, dioxygenases, oxidoreductases, and metallo-β-lactamase domain-containing proteins, showed generally moderate induction, reflecting a coordinated cellular response to oxidative stress and host-derived antimicrobial compounds.

Expression profiles of hormone-related genes implicated in host–pathogen interactions were analyzed among the selected DEGs. A subset of genes encoding putative salicylate hydroxylases, auxin transport components, and ethylene-inducing factors were differentially expressed, suggesting their involvement in modulation of host defense pathways.

Notably, multiple genes encoding putative salicylate hydroxylases (e.g., *NelutCtg15g2550.1*, *NelutCtg04g0750.1*, *NelutCtg03g1580.1*) showed elevated expression levels, supporting a potential role in suppressing salicylic acid mediated plant defenses. Among these, *NelutCtg15g2550.1* exhibited the highest expression in shoots (FC = 9.15) (Supplementary Table 1).

Additionally, *NelutCtg02g3930.1*, encoding a necrosis- and ethylene-inducing peptide 1 (NEP1)-like protein precursor, showed markedly higher expression in fruit (FC = 19.44) compared to shoots (FC = 3.13), indicating possible tissue-specific regulation (Supplementary Table 1).

Transport-related genes constituted a substantial component of the infection-responsive transcriptome, with major facilitator superfamily (MFS) transporters, ABC transporters, amino acid permeases, and siderophore-associated transporters being prominently represented. Among the most prominently expressed genes, *NelutCtg13g3610.1* (putative MFS transporter) exhibited exceptionally high expression in shoots (FC = 898.87) and remained strongly expressed in fruit (FC = 109.21), suggesting a central role in substrate transport during infection. Similarly, *NelutCtg01g8430.1* (MFS domain-containing protein) and *NelutCtg02g3480.1* (putative MFS transporter) similarly elevated expression across both tissues, emphasizing their importance in nutrient acquisition and detoxification processes (Table 1).

Mitochondrial transport machinery was significantly upregulated, with an outer mitochondrial membrane transport complex protein (*NelutCtg28g0420.1*) displaying substantial expression levels (FC = 116.51 in branches vs. 41.49 in fruit), indicating enhanced mitochondrial function and energy metabolism during host colonization.

Peptide transport capacity was augmented through upregulation of oligopeptide transporters (*NelutCtg03g1790.1*) and small oligopeptide family transporters (*NelutCtg01g5200.1*), suggesting enhanced nitrogen acquisition mechanisms that may support fungal growth in nutrient-limited host environments (Supplementary Table 1).

Table 1
List of differentially expressed genes (DEGs) exhibiting fold change (FC) > 20 in at least one infection condition.

Gene ID	Description	FC NLB vs NLPDA	FC NLF vs NLPDA	Function
NelutCtg15g0740.1	Putative pectate lyase protein	2129.81	19186.09	Cell wall hydrolysis
NelutCtg01g8260.1	Conserved hypothetical protein cutinase	103.23	27.02	Cell wall hydrolysis
NelutCtg20g1770.1	Putative glycoside hydrolase family 61 protein	71.97	805.16	Cell wall hydrolysis
NelutCtg13g3870.1	Putative glycosyl hydrolase family 7 protein	62.48	232.63	Cell wall hydrolysis
NelutCtg19g0400.1	Putative glycoside hydrolase family 61 protein	32.60	101.95	Cell wall hydrolysis
NelutCtg17g2640.1	Glycoside hydrolase subgroup catalytic core	32.51	6.06	Cell wall hydrolysis
NelutCtg10g4310.1	Glycoside hydrolase family 12	29.04	18.74	Cell wall hydrolysis
NelutCtg27g0160.1	Putative endoglucanase family 5 glycoside hydrolase protein	28.64	81.10	Cell wall hydrolysis
NelutCtg10g0470.1	Putative glycoside hydrolase family 61 protein	19.75	35.08	Cell wall hydrolysis
NelutCtg33g0210.1	Putative glycoside hydrolase family 43 protein	17.33	35.40	Cell wall hydrolysis
NelutCtg16g0800.1	Putative glycoside hydrolase family 61 protein	13.75	34.08	Cell wall hydrolysis
NelutCtg06g1640.1	Putative glycoside hydrolase family 3 protein	6.20	48.31	Cell wall hydrolysis
NelutCtg05g6050.1	Putative carbohydrate esterase family 8 protein / Pectinesterase	2.41	203.78	Cell wall hydrolysis
NelutCtg29g0320.1	Putative pisatin demethylase protein	302.32	205.81	Detoxification
NelutCtg09g0820.1	Short-chain dehydrogenase/reductase SDR	297.76	143.48	Detoxification
NelutCtg23g0410.1	Putative alpha beta-hydrolase protein	253.02	72.64	Detoxification
NelutCtg16g1270.1	Putative aldo keto reductase protein	68.43	23.40	Detoxification
NelutCtg06g5610.1	Putative antibiotic biosynthesis monooxygenase protein	68.15	53.60	Detoxification
NelutCtg29g0250.1	Putative aldo keto protein	24.00	78.00	Detoxification
NelutCtg27g0350.1	Putative peptidase m35 deuterolysin protein	399.71	1.91	Protease
NelutCtg01g0170.1	Putative peptidase s8 s53 subtilisin kexin sedolisin protein	245.38	17.86	Protease
NelutCtg18g2870.1	Putative serine protease protein	33.42	3.79	Protease
NelutCtg04g3800.1	Putative aminopeptidase Y	32.80	16.71	Protease
NelutCtg14g3410.1	Putative metalloprotease protein	6.93	22.68	Protease
NelutCtg01g3020.1	Putative fatty acid elongase (Gns1)	319.24	22.19	Stress tolerance
NelutCtg07g1700.1	Putative 30 kda heat shock protein	24.67	148.59	Stress tolerance
NelutCtg03g4730.1	Putative heat shock protein hsp98 hsp104 protein	8.72	25.34	Stress tolerance
NelutCtg02g0180.1	Putative choline dehydrogenase protein	7.35	37.95	Stress tolerance
NelutCtg27g1070.1	Putative sterigmatocystin biosynthesis monooxygenase stcW	1972.63	608.10	Toxin
NelutCtg22g1170.1	Putative sterigmatocystin biosynthesis monooxygenase stcW	251.39	90.81	Toxin
NelutCtg29g0240.1	Putative tri7-like toxin biosynthesis protein	54.53	126.92	Toxin
NelutCtg29g0270.1	Putative sterigmatocystin 8-o-methyltransferase precursor protein	36.39	35.70	Toxin
NelutCtg29g0220.1	Putative polyketide synthase protein	17.73	33.05	Toxin
NelutCtg10g0120.1	Putative Zn(II)2Cys6 transcription factor	20.31	4.02	Transcription Factor
NelutCtg13g3610.1	Putative MFS transporter protein	898.87	109.21	Transport
NelutCtg01g8430.1	MFS domain-containing protein	545.78	10.30	Transport
NelutCtg02g3480.1	Putative MFS transporter protein	407.48	254.35	Transport
NelutCtg28g0420.1	Outer mitochondrial membrane transport complex protein	116.51	41.49	Transport
NelutCtg03g1790.1	Putative oligopeptide transporter protein	75.84	37.19	Transport

Gene ID	Description	FC NLB vs NLPDA	FC NLF vs NLPDA	Function
NelutCtg19g0590.1	Putative MFS polyamine protein	62.30	43.20	Transport
NelutCtg02g2540.1	Putative MFS multidrug transporter protein	21.57	3.80	Transport

Multiple genes associated with multidrug resistance were differentially expressed, including several MFS multidrug transporters (*NelutCtg02g2540.1*, *NelutCtg04g2370.1*) and ABC transporters (*NelutCtg06g3550.1*, *NelutCtg01g7050.1*). These efflux systems likely facilitate the removal of toxic secondary metabolites and plant-derived antimicrobial compounds, thereby enhancing fungal survival and persistence within hostile host environments (Supplementary Table 1).

Iron acquisition systems were represented by siderophore-related transporters, including *NelutCtg01g0270.1* and *NelutCtg06g2630.1*, highlighting the importance of iron uptake in *N. luteum* virulence. Furthermore, the presence of sugar transporters such as *NelutCtg10g2930.1* (high-affinity glucose transporter) suggests active carbohydrate acquisition from host tissues (Supplementary Table 1).

Comprehensive analysis of stress-responsive genes revealed multiple components essential for fungal survival under host-induced stress conditions. Heat shock proteins constituted a major component of this response, with a 30 kDa heat shock protein (*NelutCtg07g1700.1*) showing particularly pronounced upregulation in fruit tissues (FC = 148.59), indicating tissue-specific stress adaptation strategies. Additional molecular chaperones, including Hsp90 (*NelutCtg03g4730.1*) and chaperonin ClpA/B (*NelutCtg14g1440.1*), exhibited high expression levels, suggesting critical roles in maintaining protein homeostasis and cellular integrity during infection (Supplementary Table 1).

Osmotic stress tolerance was potentially mediated by choline dehydrogenase genes (*NelutCtg02g0180.1*, *NelutCtg20g0650.1*, *NelutCtg01g4230.1*), which showed differential expression patterns indicative of their importance in fungal adaptation to host environments. A Bax inhibitor family protein (NelutCtg06g2560.1) was also upregulated, potentially contributing to suppression of host-induced programmed cell death pathways and thereby promoting fungal establishment and survival (Supplementary Table 1).

Transcriptional control of virulence responses was mediated by several key regulatory factors. A $Zn(II)_2Cys_6$ transcription factor (*NelutCtg10g0120.1*) exhibited strong expression (FC = 20.31), underscoring the importance of fungal-specific transcriptional regulatory networks in coordinating pathogenicity gene expression during host infection (Table 1).

Functional annotation and pathways analysis of differentially expressed genes

To characterize the infection process of *N. luteum* in susceptible avocado branches and fruits, all DEGs were functionally enriched and categorized based on gene ontology (GO) annotations.

During branch infection, DEGs were significantly enriched in biological processes (BP) with the highest EnrichRatio values observed for protein refolding (GO:0042026), cellulose metabolic process (GO:0030243), oligopeptide transport (GO:0006857), and siderophore metabolic process (GO:0009237) (Fig. 7a). These enrichments collectively suggest activation of proteostasis mechanisms under host-induced stress, degradation of plant cell wall components to facilitate tissue colonization, enhanced nutrient scavenging, and iron acquisition, a well-established determinant of fungal virulence.

During fruit infection, a distinct and metabolically intensive transcriptional program was identified (Fig. 7b). Carbohydrate and monosaccharide transmembrane transport (GO:0034219; GO:0015749) were prominently enriched, indicating enhanced sugar acquisition consistent with exploitation of the nutrient-rich fruit environment. Additionally, enrichment of glycosphingolipid metabolism (GO:0006687) suggested active membrane remodeling, while overrepresentation of multiple mitochondrial-associated processes, including protein targeting (GO:0006626), mitochondrial transport (GO:0006839), and transmembrane transport (GO:1990542), pointed to increased respiratory activity sustaining elevated metabolic demands. Finally, enrichment of xenobiotic transmembrane transport (GO:0006855) indicated activation of detoxification and efflux systems, likely enabling *N. luteum* to counteract host-derived antimicrobial compounds.

Identification of N. luteum candidate effector proteins

To identify candidate effector proteins (CEPs) involved in the pathogenesis of *N. luteum*, the CSIRO tool Effector P 3.0, a machine learning–based predictor for fungal and oomycete effectors [49], was employed. Genome-wide analysis revealed 2,745 predicted CEPs, which were classified based on their predicted subcellular localization: 2,415 (87.9%) cytoplasmic, 270 (9.8%) apoplastic, and 60 (2.2%) with potential dual localization to either compartment. Expression profiling during infection revealed that 373 CEPs (13.6%) were significantly upregulated compared to in vitro conditions. Among these infection-responsive effectors, 127 were specifically induced during branch infection, 90 during fruit infection, and 156 showed consistent upregulation in both tissue types, indicating both shared and tissue-specific virulence mechanisms. To refine this dataset, only CEPs with a prediction probability greater than 50% and detectable expression in at least one experimental condition were retained (Table 2 and Table 3). To assess potential functional similarity with previously characterized effectors, sequence comparisons were performed against the PHI-base (version 4.18), a curated database of experimentally validated pathogen–host interaction genes. BLASTp analysis was conducted using an e-value cutoff of 1.04×10^{-15} and a minimum identity threshold of 25%. This filtering resulted in the identification of 38 high-confidence CEPs. Of these, 34 (89.5%) were overexpressed under infection conditions in both branch and fruit tissues (Table 2), while four exhibited tissue-specific expression patterns: one expressed exclusively in branches and three specifically in fruit tissues (Table 3). Subcellular localization predictions revealed distinct targeting patterns: 17 CEPs were predicted to be secreted using SignalP 3.0 [50] and localized to the apoplast, facilitating direct interaction with host cell wall components and extracellular matrices. In contrast, 18 CEPs were predicted to function within

the host cytoplasm, potentially interfering with intracellular processes. Three proteins (*NelutCtg08g4740.1*, *NelutCtg02g2820.1*, and *NelutCtg15g0740.1*) exhibited predicted dual localization capacity, suggesting potential multifunctional roles across different cellular compartments during infection.

The most prominently expressed effector was a putative pectate lyase (*NelutCtg15g0740.1*), which displayed exceptionally high expression levels in both tissue types (FC = 2,129.81 in branches; FC = 19,186.08 in fruit). This dramatic upregulation, combined with its predicted cell wall-degrading activity, positions this effector as a prime candidate for mediating host tissue maceration and facilitating fungal colonization.

Table 2
Candidate effector genes upregulated during *N. luteum* infection of both fruit and branch tissues.

Gene ID	Alpahfold description	Signal peptide	PHI	Cytoplasmic prediction	Aploplastic prediction	Localization	FC NLB vs NLPDA	FC NL NL
NelutCtg10g2270.1	Putative abc multidrug protein	No	*Zymoseptoria tritici* 5.07×10^{-24}	0.873	-	Cytoplasmic	2.21	1.
NelutCtg03g5270.1	Hsp90-like protein	No	*Alternaria alternata* 1.59×10^{-23}	0.832	-	Cytoplasmic	3.87	1.
NelutCtg08g4740.1	Putative pathogenesis associated protein	No	*Colletotrichumgloeosporioides* 2.15×10^{-41}	0.799	0.752	Cytoplasmic/ apoplastic	3.14	1.
NelutCtg08g3970.1	Autophagy-related protein 9	No	*Magnaporthe oryzae* 8.04×10^{-32}	0.784	-	Cytoplasmic	2.06	2.
NelutCtg16g0510.1	Putative methyltransferase tdiE	No	*Fusarium oxysporum* 7.60×10^{-83}	0.747	-	Cytoplasmic	2.12	1.
NelutCtg27g0020.1	Secondary metabolism regulator LAE1	No	*Aspergillus carbonarius* 8.17×10^{-60}	0.717	-	Cytoplasmic	5.91	2.
NelutCtg02g2820.1	Superoxide dismutase [Cu-Zn]	No	*Botrytis cinerea* 2.83×10^{-82}	0.710	0.628	Cytoplasmic/ apoplastic	2.04	2.
NelutCtg25g0620.1	Putative benzoate 4-monooxygenase cytochrome p450 protein	No	*Verticillium dahliae* 3.78×10^{-29}	0.708	-	Cytoplasmic	4.2	1.
NelutCtg01g0450.1	Putative heat shock protein hsp88 protein	No	*Magnaporthe oryzae* 2.42×10^{-34}	0.664	-	Cytoplasmic	1.76	2.
NelutCtg04g4530.1	Mitochondrial protein import protein mas5	No	*Pseudomonas aeruginosa* 6.59×10^{-46}	0.663	-	Cytoplasmic	3.8	4.
NelutCtg03g0240.1	Uncharacterized protein	No	Botrytis cinerea 3.08 × 10–16	0.658	-	Cytoplasmic	1.30	2.
NelutCtg01g6620.1	Methyltransferase type 11	No	*Fusarium o×ysporum* 1.88×10^{-69}	0.633	-	Cytoplasmic	25.01	4.
NelutCtg05g3810.1	Catabolic 3-dehydroquinase	No	*Ralstonia solanacearum* 1.55×10^{-54}	0.625	-	Cytoplasmic	6.31	6.
NelutCtg01g0050.1	Putative homeobox and c2h2 transcription protein	No	*Magnaporthe oryzae* 6.12×10^{-36}	0.550	-	Cytoplasmic	2.22	-1
NelutCtg15g0740.1	Putative pectate lyase protein	Yes	*Fusarium solani* 1.36×10^{-68}	0.543	0.761	Cytoplasmic/ apoplastic	2129.81	19
NelutCtg01g3780.1	Putative norsolorinic acid reductase protein	No	*Aspergillus flavus* 1.53×10^{-153}	0.530	-	Cytoplasmic	2.29	2.
NelutCtg06g1310.1	Putative hsp70-like protein	No	*Magnaporthe oryzae* 5.61×10^{-35}	0.529	-	Cytoplasmic	9.33	14
NelutCtg01g0490.1	Gata transcription factor	No	*Fusarium graminearum* 1.82×10^{-58}	0.529	-	Cytoplasmic	2.33	1.

Gene ID	Alpahfold description	Signal peptide	PHI	Cytoplasmic prediction	Aploplastic prediction	Localization	FC NLB vs NLPDA	FC NI NI
NelutCtg11g1110.1	Putative heat shock protein 90 protein	No	*Fusarium graminearum* $0.00 \times 10^{+00}$	0.521	-	Cytoplasmic	5.12	6.
NelutCtg07g1890.1	Putative c2h2 transcription factor protein	No	*Botrytis cinerea* 1.02×10^{-134}	0.516	-	Cytoplasmic	2.74	2.
NelutCtg19g0220.1	Pectate lyase	Yes	*Fusarium solani* $1{,}86 \times 10^{-63}$	-	0.852	Apoplastic	34.08	21
NelutCtg16g0800.1	Putative glycoside hydrolase family 61 protein	Yes	*Magnaporthe oryzae* 6.00×10^{-35}	-	0.850	Apoplastic	13.75	34
NelutCtg08g2890.1	Putative major allergen alt protein	Yes	*Verticillium dahliae* 1.04×10^{-15}	-	0.785	Apoplastic	1.06	7.
NelutCtg06g2140.1	Pectate lyase	Yes	*Fusarium solani* 1.53×10^{-62}	-	0.767	Apoplastic	52.49	75
NelutCtg08g1640.1	Putative extracellular protein	Yes	*Fusarium graminearum* 4.42×10^{-159}	-	0.755	Apoplastic	5.90	8.
NelutCtg02g3510.1	Putative endopolygalacturonase protein	Yes	*Lasiodiplodia theobromae* 3.19×10^{-174}	-	0.730	Apoplastic	1.69	2.
NelutCtg13g3870.1	Glucanase	Yes	*Phytophthora sojae* 1.42×10^{-166}	-	0.696	Apoplastic	62.48	23
NelutCtg10g4280.1	Putative glycoside hydrolase family 12 protein	Yes	*Phytophthora sojae* 2.52×10^{-79}	-	0.663	Apoplastic	-4.77	8.
NelutCtg18g2700.1	Putative glycoside hydrolase family 61 protein	Yes	*Magnaporthe oryzae* 9.45 × 10–35	-	0.655	Apoplastic	1.84	2.
NelutCtg04g6080.1	Putative metalloprotease 1 protein	Yes	*Fusarium oxysporum* 1.02×10^{-88}	-	0.649	Apoplastic	3.35	3.
NelutCtg07g0490.1	Pectate lyase	Yes	*Fusarium graminearum* 8.98×10^{-63}	-	0.581	Apoplastic	6.58	5.
NelutCtg04g3710.1	Putative scp-like extracellular protein	Yes	*Fusarium verticillioides* 3.73×10^{-34}	-	0.558	Apoplastic	4.55	2.
NelutCtg07g6000.1	Putative pectin lyase a protein	Yes	Botrytis cinerea 4.48 × 10–115	-	0.516	Apoplastic	1.35	3.
NelutCtg03g6860.1	Pectinesterase	Yes	*Botrytis cinerea* 7.20×10^{-88}	-	0.503	Apoplastic	2.05	1.

Table 3
Candidate effector genes exhibiting tissue-specific expression during *N. luteum* infection of fruit and branch tissues

Gene ID	Alphafold description	Signal peptide	PHI	Effector prediction	Localization	Tissue
NelutCtg25g0620.1	Putative benzoate 4 monooxygenase cytochrome p450 protein.	No	*Verticillium dahliae* $3{,}78 \times 10^{-29}$	0.708	Cytoplasmic	Branch
NelutCtg02g3930.1	Putative necrosis and ethylene incucing peptide 1 protein. NPP1 domain protein,	Yes	*Phityum aphanidermatum* $1{,}82 \times 10^{-72}$	0.627	Apoplastic	Fruit
NelutCtg05g6050.1	Pectinesterase	Yes	*Botrytis cinerea* $5{,}58 \times 10^{-82}$	0.571	Apoplastic	Fruit
NelutCtg19g1370.1	Pectin lyase fold/virulence factor macrophomina pahseolina	Yes	*Magnaporthe Oryzae* $2{,}90 \times 10^{-167}$	0.546	Apoplastic	Fruit

Discussion

Neofusicoccum luteum has been widely reported in major avocado-growing regions, including California, Italy, and Spain, underscoring its global relevance [30, 51, 52]. By integrating genome sequencing with comparative transcriptomic analyses under two infection conditions (avocado branches and fruits) relative to growth on PDA, this study elucidates the molecular basis of pathogenicity and tissue-specific responses.

The assembled genome (40.82 Mb) is comparable to previously reported genome sizes for members of the Botryosphaeriaceae, including *Neofusicoccum parvum*, *Botryosphaeria dothidea*, and *Lasiodiplodia theobromae*, which typically range from 40 to 45 Mb [17–19]. Ortholog analysis revealed a large shared core genome among these four species, with 7,300 of 10,842 gene clusters conserved across all taxa (~ 67%), reflecting essential biological functions linked to pathogenicity, stress tolerance, and host colonization. This pattern is consistent with the pangenome architecture commonly described in fungal plant pathogens, where a stable core genome is complemented by a more dynamic accessory component [53]. Species-specific ortholog clusters support the role of the accessory genome in driving lineage-specific adaptation, potentially contributing to differences in host interaction, infection strategy, and aggressiveness [54]. In the context of avocado dieback in Andalusia, this genomic plasticity may help explain why multiple Botryosphaeriaceae species coexist within the same production area yet differ in frequency, symptom severity, and ecological niche occupancy [30].

The high completeness of the genome assembly, supported by the recovery of 95% complete conserved orthologs with minimal duplication and few missing genes [48, 55], provided a robust foundation for virulence factor identification [56]. Genome analysis also identified a diverse CAZyme repertoire (664 genes), with glycoside hydrolases as the most prevalent class, followed by auxiliary activity enzymes and glycosyltransferases, indicating strong capacity for plant cell wall degradation and lignocellulosic material modification [57, 58]. Comparative analysis across related species revealed a broadly conserved enzymatic distribution, consistent with previous reports of extensive CAZyme expansions in Botryosphaeriaceae associated with enhanced virulence [20, 30, 59]. Although *B. dothidea* and *L. theobromae* exhibited slightly higher total CAZyme-related gene numbers, overall class distribution remained consistent, reflecting conserved functional requirements of their pathogenic lifestyle [60, 61]. Subtle interspecific differences in CAZyme repertoires nonetheless appear associated with host adaptation, as species colonizing lignocellulosic hosts tend to show expansions in plant cell wall–degrading enzymes [62, 63].

RNA-seq analysis of *N. luteum* colonizing avocado branches and fruit revealed extensive transcriptional reprogramming relative to growth on PDA, consistent with findings in *N. parvum* during peach shoot infection and growth on grapevine wood tissue [24, 64]. Higher numbers of DEGs were detected during branch infection than during fruit infection, indicating a more extensive transcriptional response in woody tissues and aligning with the stress-responsive expression of virulence-associated genes reported in other Botryosphaeriaceae species [59].

Tissue-dependent differences were further reflected in functional enrichment patterns. Fruit infection was marked by enrichment of carbohydrate and monosaccharide transport processes, consistent with enhanced host-derived sugar acquisition. Mitochondrial functions were enriched under both conditions but likely reflect elevated metabolic activity in fruit versus energetic demands of adapting to woody host constraints in branches. Enrichment of glycosphingolipid metabolism during fruit infection points to active membrane remodeling at the host interface [65], while upregulation of xenobiotic detoxification pathways highlights the fungus's capacity to counteract host-derived antimicrobial defenses, an established feature of Botryosphaeriaceae pathogenicity [66, 67].

Among differentially expressed candidate pathogenicity-related genes, those associated with cell wall degradation, transport, and detoxification were most represented. CWDEs showed stronger induction during fruit infection overall, reflecting enhanced reliance on plant cell wall breakdown in this nutrient-rich tissue. Pectate lyase showed the highest induction of CWDE under both conditions, with substantially higher expression in fruit (FC = 19,186.09) than in branches (FC = 2,129.81). Pectate lyases are well-recognized virulence factors promoting tissue maceration and host colonization, with similar roles reported in *Verticillium dahliae* and *Fusarium sacchari* [68, 69]. Genes from glycoside hydrolase families GH61/AA9 and GH7, and carbohydrate esterase family CE8, were also markedly upregulated during fruit infection. These families are broadly linked to fungal virulence: AA9 proteins such as BcGH61 from *Botrytis cinerea* induce plant cell death [70], PsGH7a from *Phytophthora sojae* is required for full virulence [71], and CE8 esterases facilitate deacetylation of plant cell wall polysaccharides [72, 73]. Conversely, cutinase and a GH12 protein showed higher expression in branch tissue, consistent with roles in virulence and symptom development observed in *B. dothidea* and *F. sacchari* [74, 75].

Secreted proteases, notably peptidase M35 (deuterolysin) and a subtilisin-like S8/S53 protease, were more strongly induced in branch tissue, consistent with roles in host protein degradation and tissue maceration. S8/S53 subtilisins have been implicated in virulence in *Macrophomina phaseolina* [76], while M35 metalloproteases contribute to plant defense component degradation across diverse fungal pathogens [77]. Their preferential induction in branch tissue suggests protease-mediated host manipulation is especially prominent during woody tissue colonization.

Toxin biosynthesis genes were markedly induced during host infection. The sterigmatocystin biosynthesis monooxygenase (*stcW*) was predominantly induced in branch tissues, while a *tri7*-like toxin biosynthesis gene was more strongly expressed in fruit, indicating tissue-tailored recruitment of distinct biosynthetic pathways. Fungal phytotoxins contribute to pathogenicity through oxidative stress induction, membrane disruption, and inhibition of host metabolism [78–80]. Detoxification and nutrient acquisition were supported by broad upregulation of MFS transporters, ABC transporters, mitochondrial membrane transport complex proteins, and oligopeptide transporters. Both MFS and ABC transporter families are extensively documented in multidrug resistance, detoxification processes, and fungal pathogenicity, facilitating the efflux of host-derived toxic compounds and enabling adaptation to adverse host environments [81]. Functional analyses in *Botrytis cinerea* have demonstrated that MFS transporters directly confer tolerance to plant defense metabolites and are essential for full virulence expression [82]. Similarly, ABC transporters have been implicated in pathogenicity within the Botryosphaeriaceae, as exemplified by the *Neofusicoccum parvum*-walnut pathosystem, where the ABC1 transporter mediates fungal tolerance to host defensive responses during infection [22]. A notable component of this response was the induction of putative detoxification enzymes potentially involved in neutralizing host-derived antimicrobial compounds, including pisatin demethylase, short-chain dehydrogenase/reductase (SDR) proteins, aldo-keto reductases, α/β-hydrolases, and an antibiotic biosynthesis monooxygenase—enzyme classes commonly associated with the detoxification of plant phytoalexins and reactive electrophilic compounds [83].

N. luteum expressed genes potentially involved in manipulating host hormonal signaling pathways during infection. Upregulation of putative salicylate hydroxylases suggests active suppression of salicylic acid-mediated defense responses, a mechanism demonstrated in *Fusarium graminearum* where these enzymes degrade SA to attenuate host immunity [84]. Additionally, expression of a necrosis- and ethylene-inducing peptide 1-like protein (NLP) aligns with necrotrophic pathogenesis strategies, as NLPs are widely associated with host cell death induction across Dothideomycetes [85].

Among stress tolerance–related genes, fatty acid elongase GNS1 and HSP30 showed the highest induction with contrasting tissue profiles. GNS1, involved in very-long-chain fatty acid biosynthesis and membrane remodeling, was strongly induced in branch tissue (~ 14-fold higher), suggesting a prominent role in membrane adaptation to woody host constraints, consistent with reports in *Aspergillus flavus* during groundnut infection [86]. HSP30 was more strongly induced in fruit tissue (~ 6-fold higher), consistent with its role in responding to oxidative and proteotoxic stress [87]. These opposing tissue profiles reinforce the view that *N. luteum* mounts host-specific adaptive responses.

Of the 2,745 genome-wide effector candidates, 373 were differentially induced under infection conditions, of which 38 showed homology to proteins in the pathogen–host interaction database (PHI). The predicted candidates included both apoplastic and cytoplasmic proteins, suggesting *N. luteum* deploys extracellular and intracellular infection strategies consistent with effector-mediated host manipulation described in related Botryosphaeriaceae [66]. Among the most notable candidates, *NelutCtg15g0740.1*, *NelutCtg06g2140.1*, *NelutCtg19g0220.1*, and *NelutCtg07g0490.1* (classified in this study as CWDE) exhibited high expression in both branch and fruit, encoding putative apoplastic pectate lyase–like effectors with strong similarity to predicted pectate lyases of *Fusarium solani* (Table 2), whose silencing has been associated with reduced virulence [88]. *NelutCtg03g5270.1* and *NelutCtg11g1110.1* encoded Hsp90-like cytoplasmic effectors with high homology to characterized proteins from *Alternaria alternata* and *Fusarium graminearum* (Table 2). Hsp90 plays a critical role in fungal virulence by stabilizing key signaling proteins required for stress responses and host–pathogen interactions, and facilitates drug resistance emergence across diverse fungal pathogens [89–91]. Additional predicted effectors showed homology to pectin lyases, metalloproteases, and glucanases, proteins broadly implicated in host cell wall remodeling and defense interference, underscoring their potential contribution to the virulence strategy of this organism.

Conclusion

This study presents the first integrative genomic and transcriptomic characterization of *Neofusicoccum luteum*, a major causal agent of avocado dieback disease. The high-quality genome assembly, together with ortholog and CAZyme comparative analyses, reveals a broadly conserved yet adaptable pathogenicity framework within the Botryosphaeriaceae. This combination of evolutionary stability in core virulence mechanisms and species-specific genomic innovation underscores the capacity of *N. luteum* to colonize diverse host tissues. Transcriptomic profiling under two infection contexts highlights pronounced tissue-dependent transcriptional plasticity. The full-length transcriptome generated during branch and fruit colonization indicates that successful infection is mediated by a diverse suite of virulence-associated factors, including CWDEs, detoxification enzymes, stress-response proteins, toxins, transporters, and both apoplastic and cytoplasmic effectors, that likely act individually or synergistically to disrupt host defense and signaling processes. This complexity mirrors the severity and persistence of avocado dieback disease in production systems.

Further functional characterization of key virulence-related genes will be essential to elucidate how the fungus interferes with the host machinery and the development of the disease. Establishing an efficient genetic transformation system for this species represents a critical next step toward validating gene function. Overall, the genomic and transcriptomic resources generated here provide a robust foundation for future studies and will accelerate the development of targeted, evidence-based strategies for managing dieback disease in avocado.

Abbreviations

Aas
Auxiliary activities

ABC
ATP-binding cassette
BP
Biological process
BUSCO
Benchmarking Universal Single-Copy Orthologs
CAZymes
Carbohydrate-active enzymes
CBMs
Carbohydrate-binding modules
CEPs
Candidate effector proteins
CEs
Carbohydrate esterases
CWDE
Cell wall degrading enzymes
DEG
Differentially expressed genes
FC
Fold change
GO
Gene ontology
GHs
Glycoside hydrolases
GTs
Glycosyltransferases
NLB
N. luteum strain UMAF A1963 during colonization of susceptible 'Hass' avocado branches
NLF
N. luteum strain UMAF A1963 during colonization of susceptible 'Hass' avocado branches
NLPDA
N. luteum strain UMAF A1963 growth under in vitro conditions on potato dextrose agar
PCA
Principal component analysis
PDA
Potato dextrose agar
PLs
Polysaccharide lyases
PHI
Pathogen host interactions
SDR
Short-chain dehydrogenase/reductase
TPM
Transcripts per Million

Declarations

Ethics approval and consent to participate

Not applicable.

Consent for publication

Not applicable.

Competing interests

The authors declare that they have no competing interests

Funding

This work was developed within the framework of project INV2023.014, co-financed (80%) by the European Regional Development Fund through the Andalusia ERDF 2021–2027 Programme. This study was also supported by the Spanish Ministry of Science, Innovation and Universities and the State Research Agency (MICIU/AEI/10.13039/501100011033), together with ERDF/EU funds (PID2021-125805OA-I00), and by the Spanish Recovery, Transformation and Resilience Plan funded by the European Union – NextGenerationEU (CNS2023-144643). Additional support was provided by the Consejo Superior de Investigaciones Científicas (CSIC) and MICIU/AEI through a JAE-PRE contract (JAE-PRE23-15), as well as by the European Union NextGenerationEU funds through the Momentum CSIC Programme: Develop Your Digital Talent (MMT24-IHSM-01).

DFZ was hired under the Generation D initiative promoted by Red.es, an organization attached to the Spanish Ministry for Digital Transformation and the Civil Service, aimed at attracting and retaining talent through grants and training contracts financed by the European Union NextGenerationEU Recovery, Transformation and Resilience Plan (MMT24-IHSM-01).

The funding bodies had no role in the design of the study; in the collection, analysis, or interpretation of data; or in writing the manuscript.

Author Contribution

CP planed and designed the experiments and obtained the funding. BSC, ELG, AMP, NFP and CP conducted the experiments, collected and analyzed the data. BSC, ELG, NFP, EAD, LGM, FMC and CP prepared the draft. DFZ implemented the data in AvoBase. BSC, ELP, NFP and CP wrote, reviewed and edited the manuscript. All authors read and approved the final manuscript.

Acknowledgements

Not applicable.

Availability of data and materials

The data from this study are available from the NCBI WGS PRJNA1295729, NCBI SRA PRJNA1295732 and at the AvoBase downloads section.

References

1. McDonald V, Lynch S, Eskalen A. First Report of *Neofusicoccum australe, N. luteum*, and *N. parvum* Associated With Avocado Branch Canker in California. Plant Disease. 2009;93(9):967–967. 10.1094/PDIS-93-9-0967B
2. Chebil S, Fersi R, Yakoub A, Chenenaoui S, Chattaoui M, Melki I, et al. First Report of *Botryosphaeria dothidea, Diplodia seriata*, and *Neofusicoccum luteum* Associated with Canker and Dieback of Grapevines in Tunisia. Plant Dis. 2014;98(3):420–420. 10.1094/PDIS-05-13-0530-PDN.
3. Fernandes L, Paiva D, Roxo I, Trovão J, Bragança H, Portugal A. First Report of *Neofusicoccum luteum* as the Causal Agent of Canker and Die-Back of *Cupressus sempervirens*. Silva Lusitana. 2021;29(2):101–14. 10.1051/silu/20212902101.
4. Urbez-Torres JR. The status of Botryosphaeriaceae species infecting grapevines. Phytopathologia Mediterranea. 2011;50(4):5–45. 10.14601/Phytopathol_Mediterr-9316.
5. Linaldeddu BT, Deidda A, Scanu B, Franceschini A, Serra S, Berraf-Tebbal A, et al. Diversity of Botryosphaeriaceae species associated with grapevine and other woody hosts in Italy, Algeria and Tunisia, with descriptions of *Lasiodiplodia exigua* and *Lasiodiplodia mediterranea sp*. nov. Fungal Divers. 2015;71(1):201–14. 10.1007/s13225-014-0301-x.
6. Tapia L, Larach A, Riquelme N, Guajardo J, Besoain X. First Report of *Neofusicoccum luteum* Causing Stem-End Rot Disease on Avocado Fruits in Chile. Plant Dis. 2020;104(7):2027–2027. 10.1094/PDIS-11-19-2299-PDN.
7. Malandrakis AA, Kissandraki M, Mikalef L, Ntougias S, Kavroulakis N. First Record of *Neofusicoccum luteum* and *Colletotrichum gloeosporioides* Causing Anthracnose and Stem End Rot on Avocado Fruits in Greece. Plant Dis. 2023;107(10):3308. 10.1094/PDIS-05-23-1008-PDN.
8. Hernández D, García-Pérez O, Perera S, González-Carracedo MA, Rodríguez-Pérez A, Siverio F. Fungal Pathogens Associated with Aerial Symptoms of Avocado (Persea americana Mill.) in Tenerife (Canary Islands, Spain) Focused on Species of the Family Botryosphaeriaceae. Microorganisms. 2023;11(3):585. 10.3390/microorganisms11030585.
9. Arjona-Girona I, Ruano-Rosa D, López-Herrera CJ. Identification, pathogenicity and distribution of the causal agents of dieback in avocado orchards in Spain. Span J Agric Res. 2019;17(1):e1003. 10.5424/sjar/2019171-13561.
10. Baskarathevan J, Jaspers MV, Jones EE, Ridgway HJ. Development of isolate-specific markers for *Neofusicoccum parvum* and *N. luteum* and their use to study rainwater splash dispersal in the vineyard. Plant Pathol. 2013;62(3):501–9. 10.1111/j.1365-3059.2012.02675.x.
11. Mohankumar V, Dann EK, Akinsanmi OA. Seasonal dynamics of inoculum of Botryosphaeriaceae in macadamia orchards in Australia. Plant Pathol. 2023;72(6):1160–70. 10.1111/ppa.13730.
12. Marsberg A, Kemler M, Jami F, Nagel JH, Postma-Smidt A, Naidoo S, et al. *Botryosphaeria dothidea*: a latent pathogen of global importance to woody plant health. Mol Plant Pathol. 2017;18(4):477–88. 10.1111/mpp.12495.

13. Amponsah NT, Jones EE, Ridgway HJ, Jaspers MV. Factors affecting *Neofusicoccum luteum* infection and disease progression in grapevines. Australasian Plant Pathol. 2014;43(5):547–56. 10.1007/s13313-014-0294-7.
14. Möller H, Slippers B, Van Den Berg N. Branch canker battles: understanding and managing the Botryosphaeriaceae in avocado. Phytoparasitica. 2025;53(1):17. 10.1007/s12600-024-01227-6.
15. Consejería, de Agricultura. Accessed, Pesca, Agua y Desarrollo Rural de la Junta de Andalucía. Síntomas y métodos de control del hongo descendente del aguacate [Internet]. 29 June 2022. RAIF. Available from: https://juntadeandalucia.es/agriculturapescaaguaydesarrollorural/raif/sintomas-y-metodos-de-control-del-hongo-descendente-del-aguacate/. 2025 Aug 1.
16. TROPS. La enfermedad de la seca de rama en aguacate [Internet]. March 2023. Technical Department of TROPS in collaboration with IHSM-UMA/CSIC, Viveros Brokaw España, and Viveros Blanco. Available from: https://www.trops.es/wp-content/uploads/2023/03/BOLETIN-LA-SECA-DE-RAMA-EN-AGUACATE-2023.pdf. Accessed 2025 Aug 1.
17. Liu Z, Lian S, Li B, Lu H, Dong X, Wang C. Draft Genome Sequence of *Botryosphaeria dothidea*, the Pathogen of Apple Ring Rot. Genome Announc. 2016;4(5):e01142–16. 10.1128/genomeA.01142-16.
18. Ali SS, Asman A, Shao J, Balidion JF, Strem MD, Puig AS, et al. Genome and transcriptome analysis of the latent pathogen *Lasiodiplodia theobromae*, an emerging threat to the cacao industry. Genome. 2020;63(1):37–52. 10.1139/gen-2019-0112.
19. Blanco-Ulate B, Rolshausen P, Cantu D. Draft Genome Sequence of *Neofusicoccum parvum* Isolate UCR-NP2, a Fungal Vascular Pathogen Associated with Grapevine Cankers. Genome Announc. 2013;1(3):e00339–13. 10.1128/genomeA.00339-13.
20. Belair M, Restrepo-Leal JD, Praz C, Fontaine F, Rémond C, Fernandez O, et al. Botryosphaeriaceae gene machinery: Correlation between diversity and virulence. Fungal Biology. 2023;127(5):1010–31. 10.1016/j.funbio.2023.03.004.
21. Salvatore MM, Alves A, Andolfi A. Secondary Metabolites Produced by Neofusicoccum Species Associated with Plants: A Review. Agriculture. 2021;11(2):149. 10.3390/agriculture11020149.
22. Chen J, Han S, Li S, Wang M, Zhu H, Qiao T, et al. Comparative Transcriptomics and Gene Knockout Reveal Virulence Factors of *Neofusicoccum parvum* in Walnut. Front Microbiol. 2022;13:926620. 10.3389/fmicb.2022.926620.
23. Fillat Ú, Martín-Sampedro R, Macaya-Sanz D, Martín JA, Ibarra D, Martínez MJ, et al. Screening of eucalyptus wood endophytes for laccase activity. Process Biochem. 2016;51(5):589–98. 10.1016/j.procbio.2016.02.006.
24. Zhang Y, Liu Y, Gan Z, Du W, Ai X, Zhu W, et al. Transcriptomic and sugar metabolic analysis reveals molecular mechanisms of peach gummosis in response to *Neofusicoccum parvum* infection. Front Plant Sci. 2024;15:1478055. 10.3389/fpls.2024.1478055.
25. White TJ, Bruns T, Lee S, Taylor J, AMPLIFICATION AND DIRECT SEQUENCING OF FUNGAL RIBOSOMAL RNA GENES E. 1990 [cited 2026 May 14]. pp. 315–22. Available from: https://linkinghub.elsevier.com/retrieve/pii/B9780123721808500421 10.1016/B978-0-12-372180-8.50042-1
26. Carbone I, Kohn LM. A method for designing primer sets for speciation studies in filamentous ascomycetes. Mycologia. 1999;91(3):553–6. 10.1080/00275514.1999.12061051.
27. Glass NL, Donaldson GC. Development of primer sets designed for use with the PCR to amplify conserved genes from filamentous ascomycetes. Appl Environ Microbiol. 1995;61(4):1323–30. 10.1128/aem.61.4.1323-1330.1995.
28. Liu YJ, Whelen S, Hall BD. Phylogenetic relationships among ascomycetes: evidence from an RNA polymerase II subunit. Mol Biol Evol. 1999;16(12):1799–808. 10.1093/oxfordjournals.molbev.a026092.
29. Nagel JH, Wingfield MJ, Slippers B. Next-generation sequencing provides important insights into the biology and evolution of the Botryosphaeriaceae. Fungal Biology Reviews. 2021;38:25–43. 10.1016/j.fbr.2021.09.002.
30. Crespo M, Guirado-Manzano L, Sarmiento D, Guirado E, De Vicente A, Fernández-Ortuño D, et al. Fungal Species of Botryosphaeriaceae Associated With Avocado Dieback in Southern Spain. Plant Pathol. 2026;75(1):e70079. 10.1111/ppa.70079.
31. Healey A, Furtado A, Cooper T, Henry RJ. Protocol: a simple method for extracting next-generation sequencing quality genomic DNA from recalcitrant plant species. Plant Methods. 2014;10:21. 10.1186/1746-4811-10-21.
32. Li R, Li Y, Kristiansen K, Wang J. SOAP: short oligonucleotide alignment program. Bioinformatics. 2008;24(5):713–4. 10.1093/bioinformatics/btn025.
33. Bankevich A, Nurk S, Antipov D, Gurevich AA, Dvorkin M, Kulikov AS, et al. SPAdes: A New Genome Assembly Algorithm and Its Applications to Single-Cell Sequencing. J Comput Biol. 2012;19(5):455–77. 10.1089/cmb.2012.0021.
34. Simpson JT, Wong K, Jackman SD, Schein JE, Jones SJM, Birol I. ABySS: a parallel assembler for short read sequence data. Genome Res. 2009;19(6):1117–23. 10.1101/gr.089532.108.
35. Lin SH, Liao YC. CISA: contig integrator for sequence assembly of bacterial genomes. PLoS ONE. 2013;8(3):e60843. 10.1371/journal.pone.0060843.
36. Ter-Hovhannisyan V, Lomsadze A, Chernoff YO, Borodovsky M. Gene prediction in novel fungal genomes using an ab initio algorithm with unsupervised training. Genome Res. 2008;18(12):1979–90. 10.1101/gr.081612.108.
37. Manni M, Berkeley MR, Seppey M, Simão FA, Zdobnov EM. BUSCO Update: Novel and Streamlined Workflows along with Broader and Deeper Phylogenetic Coverage for Scoring of Eukaryotic, Prokaryotic, and Viral Genomes. Kelley J, editor. Molecular Biology and Evolution. 2021;38(10):4647–54. 10.1093/molbev/msab199
38. Fernandez-Pozo N, Bombarely A. EasyGDB: a low-maintenance and highly customizable system to develop genomics portals. Bioinformatics. 2022;38(16):4048–50. 10.1093/bioinformatics/btac412.
39. Ewels P, Magnusson M, Lundin S, Käller M. MultiQC: summarize analysis results for multiple tools and samples in a single report. Bioinformatics. 2016;32(19):3047–8. 10.1093/bioinformatics/btw354.

40. Bolger AM, Lohse M, Usadel B. Trimmomatic: a flexible trimmer for Illumina sequence data. Bioinformatics. 2014;30(15):2114–20. 10.1093/bioinformatics/btu170.
41. Kim D, Paggi JM, Park C, Bennett C, Salzberg SL. Graph-based genome alignment and genotyping with HISAT2 and HISAT-genotype. Nat Biotechnol. 2019;37(8):907–15. 10.1038/s41587-019-0201-4.
42. Danecek P, Bonfield JK, Liddle J, Marshall J, Ohan V, Pollard MO, et al. Twelve years of SAMtools and BCFtools. GigaScience. 2021;10(2):giab008. 10.1093/gigascience/giab008.
43. Liao Y, Smyth GK, Shi W. featureCounts: an efficient general purpose program for assigning sequence reads to genomic features. Bioinformatics. 2014;30(7):923–30. 10.1093/bioinformatics/btt656.
44. Robinson MD, McCarthy DJ, Smyth GK. edgeR: a Bioconductor package for differential expression analysis of digital gene expression data. Bioinformatics. 2010;26(1):139–40. 10.1093/bioinformatics/btp616.
45. Love MI, Huber W, Anders S. Moderated estimation of fold change and dispersion for RNA-seq data with DESeq2. Genome Biol. 2014;15(12):550. 10.1186/s13059-014-0550-8.
46. Buchfink B, Xie C, Huson DH. Fast and sensitive protein alignment using DIAMOND. Nat Methods. 2015;12(1):59–60. 10.1038/nmeth.3176.
47. Wu T, Hu E, Xu S, Chen M, Guo P, Dai Z, et al. clusterProfiler 4.0: A universal enrichment tool for interpreting omics data. Innov. 2021;2(3):100141. 10.1016/j.xinn.2021.100141.
48. Simão FA, Waterhouse RM, Ioannidis P, Kriventseva EV, Zdobnov EM. BUSCO: assessing genome assembly and annotation completeness with single-copy orthologs. Bioinformatics. 2015;31(19):3210–2. 10.1093/bioinformatics/btv351.
49. Sperschneider J, Dodds PN. EffectorP 3.0: Prediction of Apoplastic and Cytoplasmic Effectors in Fungi and Oomycetes. Mol Plant Microbe Interact. 2022;35(2):146–56. 10.1094/MPMI-08-21-0201-R.
50. Dyrløv Bendtsen J, Nielsen H, von Heijne G, Brunak S. Improved Prediction of Signal Peptides: SignalP 3.0. J Mol Biol. 2004;340(4):783–95. 10.1016/j.jmb.2004.05.028.
51. McDonald V, Eskalen A. Botryosphaeriaceae Species Associated with Avocado Branch Cankers in California. Plant Dis. 2011;95(11):1465–73. 10.1094/PDIS-02-11-0136.
52. Fiorenza A, Gusella G, Vecchio L, Aiello D, Polizzi G. Diversity of Botryosphaeriaceae species associated with canker and dieback of avocado (Persea americana) in Italy. Phytopathol Mediterr. 2023;62(1):47–63. 10.36253/phyto-14057.
53. McCarthy CGP, Fitzpatrick DA. Pan-genome analyses of model fungal species. Microb Genomics. 2019;5(2). 10.1099/mgen.0.000243.
54. Dong S, Raffaele S, Kamoun S. The two-speed genomes of filamentous pathogens: waltz with plants. Curr Opin Genet Dev. 2015;35:57–65. 10.1016/j.gde.2015.09.001.
55. Seppey M, Manni M, Zdobnov EM. BUSCO: Assessing Genome Assembly and Annotation Completeness. Methods Mol Biol. 2019;1962:227–45. 10.1007/978-1-4939-9173-0_14.
56. Möller M, Stukenbrock EH. Evolution and genome architecture in fungal plant pathogens. Nat Rev Microbiol. 2017;15(12):756–71. 10.1038/nrmicro.2017.76.
57. Kubicek CP, Starr TL, Glass NL. Plant Cell Wall–Degrading Enzymes and Their Secretion in Plant-Pathogenic Fungi. Annu Rev Phytopathol. 2014;52(1):427–51. 10.1146/annurev-phyto-102313-045831.
58. Rafiei V, Vélëz H, Tzelepis G. The Role of Glycoside Hydrolases in Phytopathogenic Fungi and Oomycetes Virulence. Int J Mol Sci. 2021;22(17):9359. 10.3390/ijms22179359.
59. Nagel JH, Wingfield MJ, Slippers B. Increased abundance of secreted hydrolytic enzymes and secondary metabolite gene clusters define the genomes of latent plant pathogens in the Botryosphaeriaceae. BMC Genomics. 2021;22(1):589. 10.1186/s12864-021-07902-w.
60. Zhao Z, Liu H, Wang C, Xu JR. Comparative analysis of fungal genomes reveals different plant cell wall degrading capacity in fungi. BMC Genomics. 2013;14(1):274. 10.1186/1471-2164-14-274.
61. Kandemir H, Peng M, Koster M, Groenewald JZ, Crous PW, Steindorff AS, et al. CAZome comparison in relation to host plant for selected Sordariomycete and Dothidiomycete plant pathogenic fungi. Front Fungal Biol. 2026;7:1789997. 10.3389/ffunb.2026.1789997.
62. Floudas D, Binder M, Riley R, Barry K, Blanchette RA, Henrissat B, et al. The Paleozoic Origin of Enzymatic Lignin Decomposition Reconstructed from 31 Fungal Genomes. Science. 2012;336(6089):1715–9. 10.1126/science.1221748.
63. Ohm RA, Feau N, Henrissat B, Schoch CL, Horwitz BA, Barry KW et al. Diverse Lifestyles and Strategies of Plant Pathogenesis Encoded in the Genomes of Eighteen Dothideomycetes Fungi. Andrianopoulos A, editor. PLoS Pathog. 2012;8(12):e1003037. 10.1371/journal.ppat.1003037
64. Massonnet M, Morales-Cruz A, Figueroa-Balderas R, Lawrence DP, Baumgartner K, Cantu D. Condition-dependent co-regulation of genomic clusters of virulence factors in the grapevine trunk pathogen *Neofusicoccum parvum*. Mol Plant Pathol. 2018;19(1):21–34. 10.1111/mpp.12491.
65. Huber A, Oemer G, Malanovic N, Lohner K, Kovács L, Salvenmoser W, et al. Membrane Sphingolipids Regulate the Fitness and Antifungal Protein Susceptibility of *Neurospora crassa*. Front Microbiol. 2019;10:605. 10.3389/fmicb.2019.00605.
66. Yan JY, Zhao WS, Chen Z, Xing QK, Zhang W, Chethana KWT, et al. Comparative genome and transcriptome analyses reveal adaptations to opportunistic infections in woody plant degrading pathogens of Botryosphaeriaceae. DNA Res. 2018;25(1):87–102. 10.1093/dnares/dsx040.
67. Belair M, Grau AL, Chong J, Tian X, Luo J, Guan X, et al. Pathogenicity Factors of Botryosphaeriaceae Associated with Grapevine Trunk Diseases: New Developments on Their Action on Grapevine Defense Responses. Pathogens. 2022;11(8):951. 10.3390/pathogens11080951.
68. Yang Y, Zhang Y, Li B, Yang X, Dong Y, Qiu D. A *Verticillium dahliae* Pectate Lyase Induces Plant Immune Responses and Contributes to Virulence. Front Plant Sci. 2018;9:1271. 10.3389/fpls.2018.01271.

69. Wang C, Huang Z, Duan Z, Zhu L, Di R, Bao Y et al. Pectate Lyase from *Fusarium sacchari* Induces Plant Immune Responses and Contributes to Virulence. Burbank LP, editor. Microbiol Spectr. 2023;11(3):e00165-23. 10.1128/spectrum.00165-23
70. Zhu W, Wang Z, Zheng C, Fang M, Huang B, Nie X, et al. Secreted Glycoside Hydrolase BcGH61 From *Botrytis cinerea* Induces Cell Death by the Apoplastic Location and Triggers Intracellular Immune Perception. Mol Plant Pathol. 2026;27(1):e70199. 10.1111/mpp.70199.
71. Tan X, Hu Y, Jia Y, Hou X, Xu Q, Han C, et al. A Conserved Glycoside Hydrolase Family 7 Cellobiohydrolase PsGH7a of *Phytophthora sojae* Is Required for Full Virulence on Soybean. Front Microbiol. 2020;11:1285. 10.3389/fmicb.2020.01285.
72. Zhu W, Wang L, Li H, Shi Y, Chang J, Wang S, et al. Whole-Genome Identification and Analysis of Carbohydrate Esterase Gene Family in *Colletotrichum graminicola*. Agriculture. 2025;15(7):781. 10.3390/agriculture15070781.
73. Wang ZM, Wang ZQ, Yuan HX, Liu MJ, Chen C, Kang JG, et al. Genomic and Functional Analysis of Carbohydrate Esterases in the Maize Pathogen *Exserohilum rostratum*. Microorganisms. 2025;13(11):2588. 10.3390/microorganisms13112588.
74. Dong BZ, Zhu XQ, Fan J, Guo LY. The Cutinase Bdo_10846 Play an Important Role in the Virulence of *Botryosphaeria dothidea* and in Inducing the Wart Symptom on Apple Plant. Int J Mol Sci. 2021;22(4):1910. 10.3390/ijms22041910.
75. Wu D, Hong T, Wang L, Ren Q, Wang S, Bao Y, et al. A *Fusarium sacchari* Glycoside Hydrolase 12 Protein FsEG1 Is a Major Virulence Factor During Sugarcane Infection and Confers Resistance to Pokkah Boeng Disease via the HIGS Strategy. Plant Biotechnol J. 2026;24(5):3458–78. 10.1111/pbi.70577.
76. Sinha N, Patra SK, Ghosh S. Secretome Analysis of *Macrophomina phaseolina* Identifies an Array of Putative Virulence Factors Responsible for Charcoal Rot Disease in Plants. Front Microbiol. 2022;13:847832. 10.3389/fmicb.2022.847832.
77. Rocha VD, Dal'Sasso TCS, Costa MDBL, De Oliveira LO. Evolutionary History and Diversification of M35 Metalloproteases in Dothideomycetes: A Phylogenomic Overview and Case Study in *Corynespora cassiicola*. Curr Microbiol. 2026;83(4):204. 10.1007/s00284-026-04772-x.
78. Xu D, Xue M, Shen Z, Jia X, Hou X, Lai D, et al. Phytotoxic Secondary Metabolites from Fungi. Toxins. 2021;13(4):261. 10.3390/toxins13040261.
79. Keller NP, Watanabe CMH, Kelkar HS, Adams TH, Townsend CA. Requirement of Monooxygenase-Mediated Steps for Sterigmatocystin Biosynthesis by *Aspergillus nidulans*. Appl Environ Microbiol. 2000;66(1):359–62. 10.1128/AEM.66.1.359-362.2000.
80. Proctor RH, McCormick SP, Kim HS, Cardoza RE, Stanley AM, Lindo L et al. Evolution of structural diversity of trichothecenes, a family of toxins produced by plant pathogenic and entomopathogenic fungi. Keller NP, editor. PLoS Pathog. 2018;14(4):e1006946. 10.1371/journal.ppat.1006946
81. Perlin MH, Andrews J, Toh SS. Essential letters in the fungal alphabet: ABC and MFS transporters and their roles in survival and pathogenicity. Adv Genet. 2014;85:201–53. 10.1016/B978-0-12-800271-1.00004-4.
82. Vela-Corcía D, Aditya Srivastava D, Dafa-Berger A, Rotem N, Barda O, Levy M. MFS transporter from *Botrytis cinerea* provides tolerance to glucosinolate-breakdown products and is required for pathogenicity. Nat Commun. 2019;10(1):2886. 10.1038/s41467-019-10860-3.
83. Müller A, Mäkelä MR, De Vries RP. Aldo-keto reductases, short chain dehydrogenases/reductases, and zinc-binding dehydrogenases are key players in fungal carbon metabolism. In: Advances in Applied Microbiology [Internet]. Elsevier; 2025 [cited 2026 May 14]. pp. 123–57. Available from: https://linkinghub.elsevier.com/retrieve/pii/S0065216424000698 10.1016/bs.aambs.2024.11.004
84. Hao G, Naumann TA, Vaughan MM, McCormick S, Usgaard T, Kelly A, et al. Characterization of a *Fusarium graminearum* salicylate hydroxylase. Front Microbiol. 2019;9:3219. 10.3389/fmicb.2018.03219.
85. Dal'Sasso TCS, Rody HVS, Oliveira LO. Genome-Wide Analysis and Evolutionary History of the Necrosis- and Ethylene-Inducing Peptide 1-Like Protein (NLP) Superfamily Across the Dothideomycetes Class of Fungi. Curr Microbiol. 2022;80(1):44. 10.1007/s00284-022-03125-8.
86. Nayak SN, Agarwal G, Pandey MK, Sudini HK, Jayale AS, Purohit S, et al. *Aspergillus flavus* infection triggered immune responses and host-pathogen cross-talks in groundnut during in-vitro seed colonization. Sci Rep. 2017;7(1):9659. 10.1038/s41598-017-09260-8.
87. Tiwari S, Thakur R, Shankar J. Role of Heat-Shock Proteins in Cellular Function and in the Biology of Fungi. Biotechnol Res Int. 2015;2015:1–11. 10.1155/2015/132635.
88. Rogers LM, Kim YK, Guo W, González-Candelas L, Li D, Kolattukudy PE. Requirement for either a host- or pectin-induced pectate lyase for infection of *Pisum sativum* by *Nectria hematococca*. Proc Natl Acad Sci USA. 2000;97(17):9813–8. 10.1073/pnas.160271497.
89. Cowen LE. Hsp90 orchestrates stress response signaling governing fungal drug resistance. PLoS Pathog. 2009;5(8):e1000471. 10.1371/journal.ppat.1000471.
90. Bui DC, Lee Y, Lim JY, Fu M, Kim JC, Choi GJ, et al. Heat shock protein 90 is required for sexual and asexual development, virulence, and heat shock response in *Fusarium graminearum*. Sci Rep. 2016;6(1):28154. 10.1038/srep28154.
91. Lamoth F, Juvvadi PR, Fortwendel JR, Steinbach WJ. Heat Shock Protein 90 Is Required for Conidiation and Cell Wall Integrity in *Aspergillus fumigatus*. Eukaryot Cell. 2012;11(11):1324–32. 10.1128/EC.00032-12.

Figures

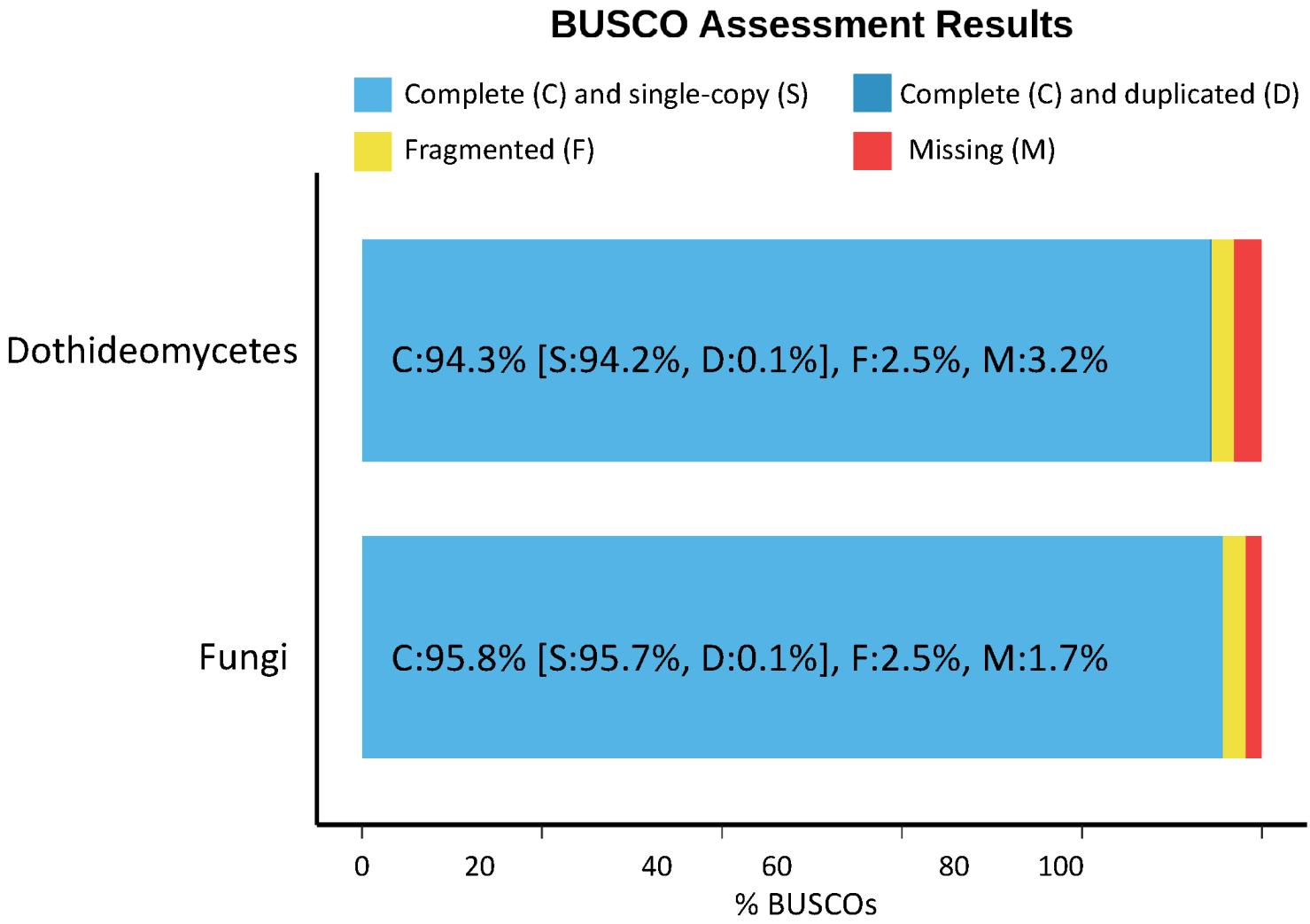


Figure 1

Benchmarking Universal Single-Copy Orthologous (BUSCO) scores. Analysis for the completeness of *N. luteum* genome assembly using the BUSCO Fungi odb10 and Dothideomycetes odb10 datasets.

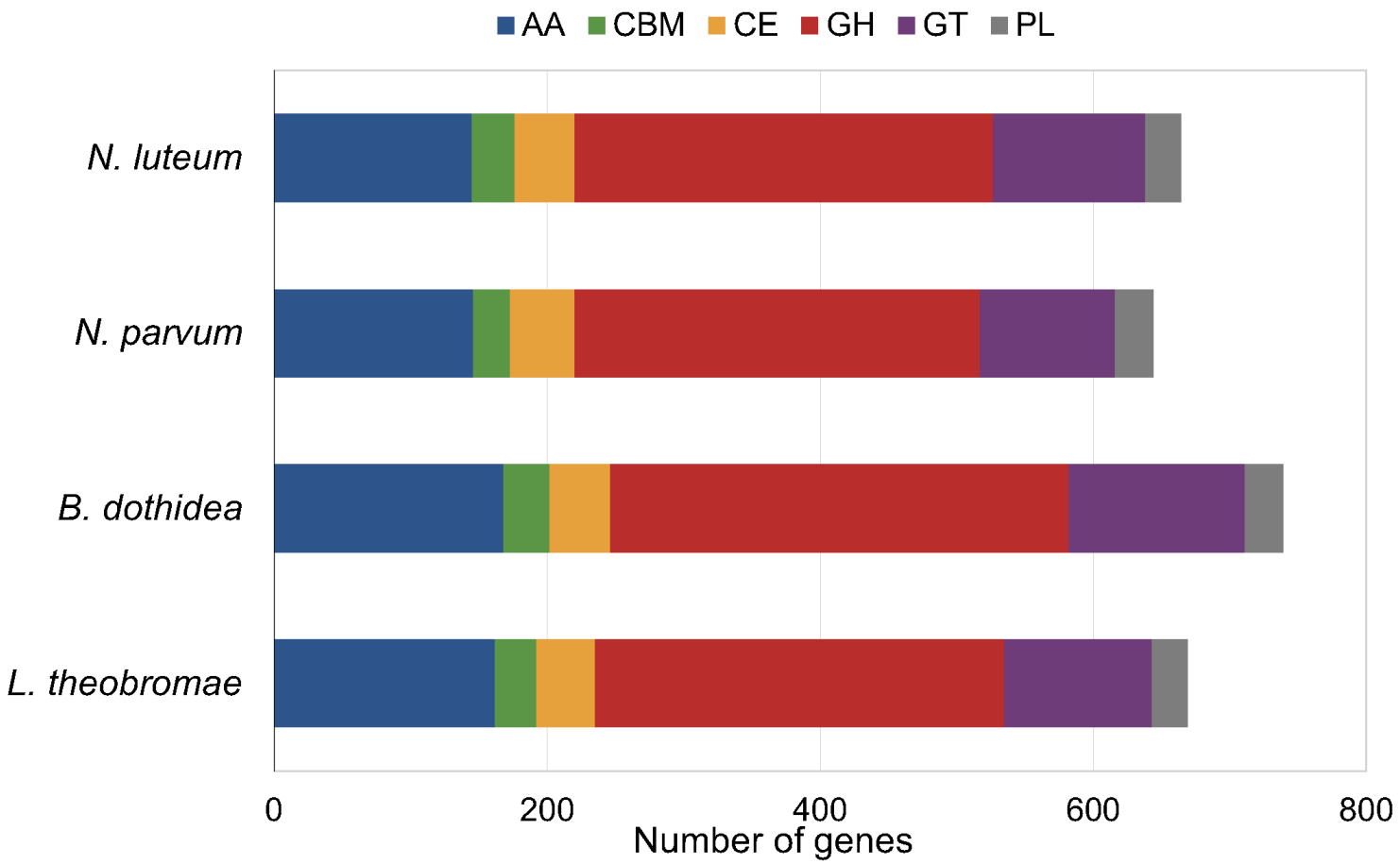


Figure 2

Carbohydrate-active enzyme (CAZyme) repertoires across major Botryosphaeriaceae dieback pathogens. Distribution of CAZyme families in *N. luteum*, *N. parvum*, *B. dothidea*, and *L. theobromae*. Colors represent different CAZyme classes: auxiliary activities (AA, blue), carbohydrate-binding modules (CBM, green), carbohydrate esterases (CE, yellow), glycoside hydrolases (GH, red), glycosyltransferases (GT, purple), and polysaccharide lyases (PL, grey).

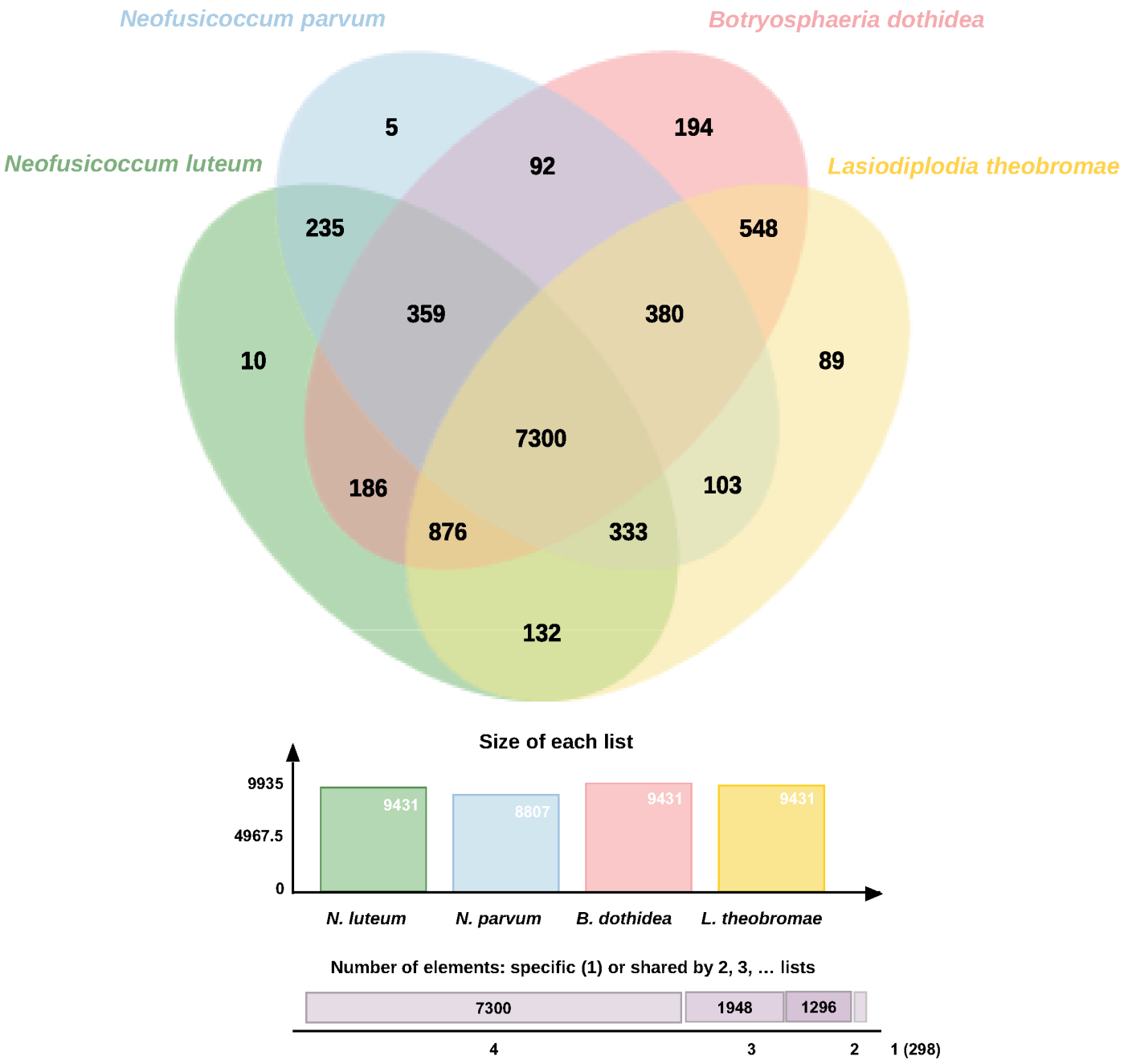


Figure 3

Orthologous gene cluster analysis among major Botryosphaeriaceae dieback pathogens. Venn diagram illustrating unique and shared orthologous gene clusters between *Neofusicoccum luteum*, *N. parvum*, *Botryosphaeria dothidea*, and *Lasiodiplodia theobromae*, with accompanying bar chart quantifying cluster numbers for each species.

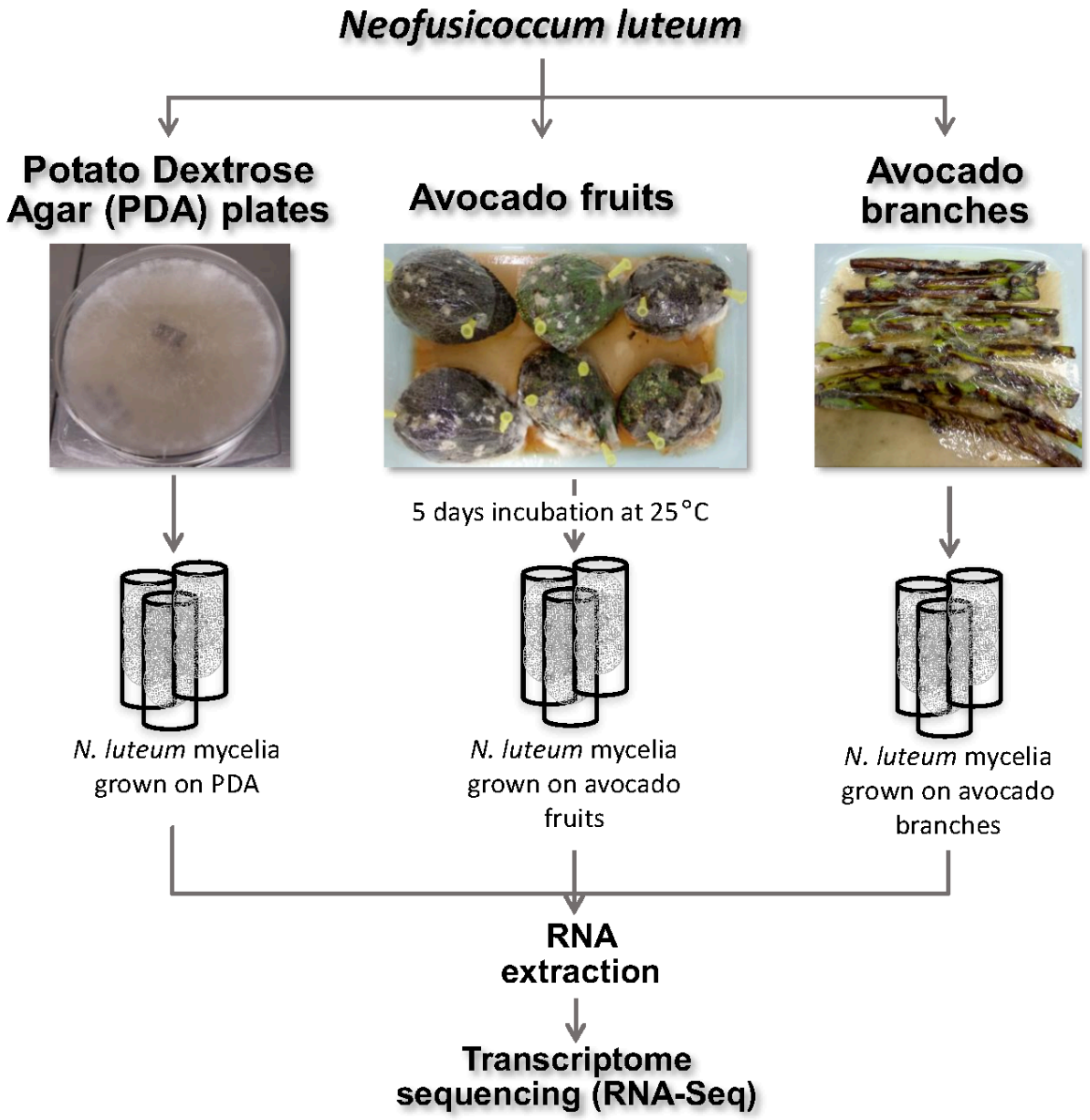


Figure 4

Experimental design for comparative transcriptome analysis. Schematic representation of *N. luteum* transcriptome analysis under three growth conditions: potato dextrose agar (PDA) medium, avocado fruits, and avocado branches.

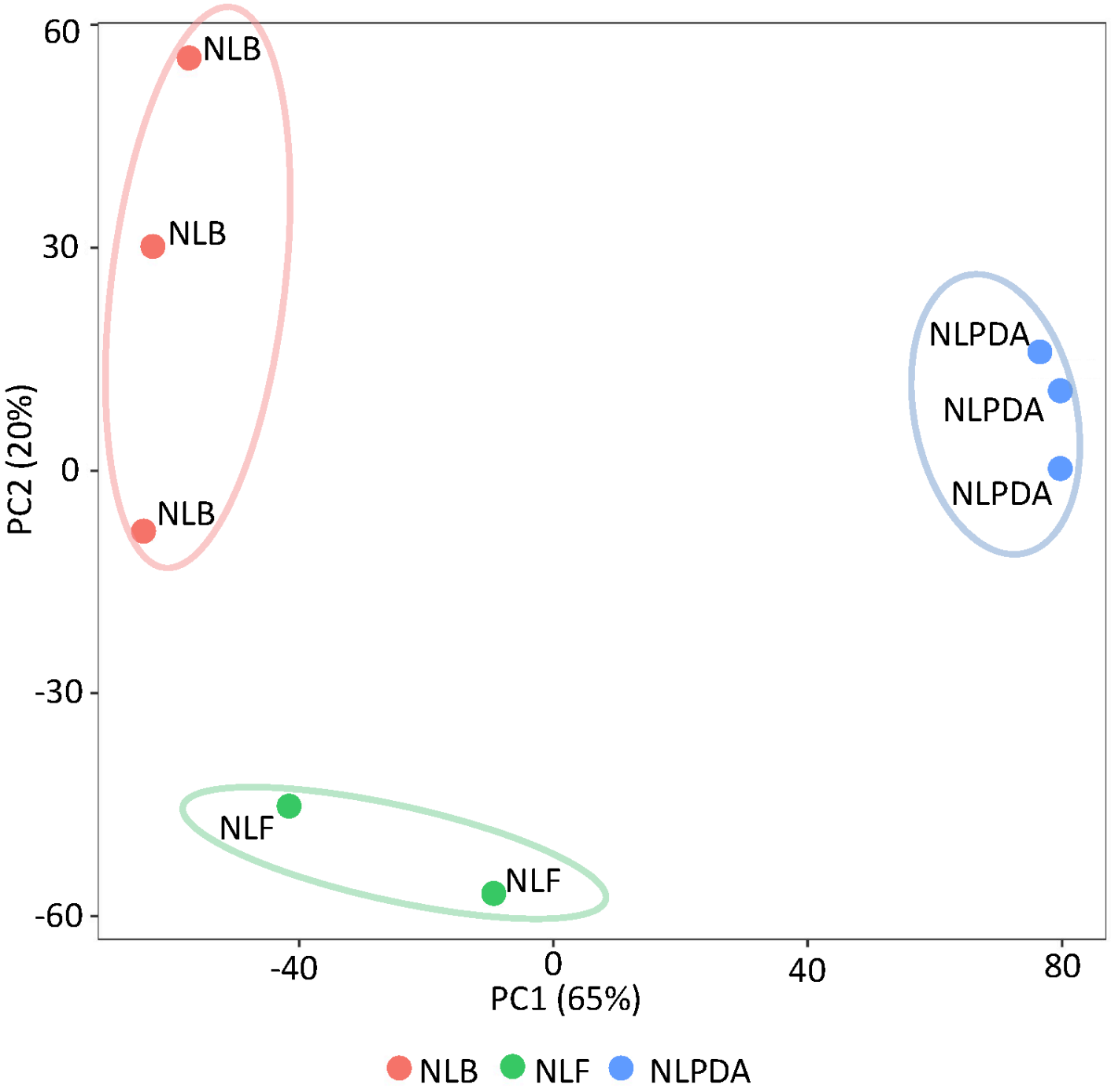


Figure 5

Principal component analysis of *N. luteum* transcriptomes across growth conditions. PC1 explains 65% of variance and PC2 explains 20% of variance. NLB: *N. luteum* on avocado branches; NLF: *N. luteum* on avocado fruits; NLPDA: *N. luteum* on PDA medium.

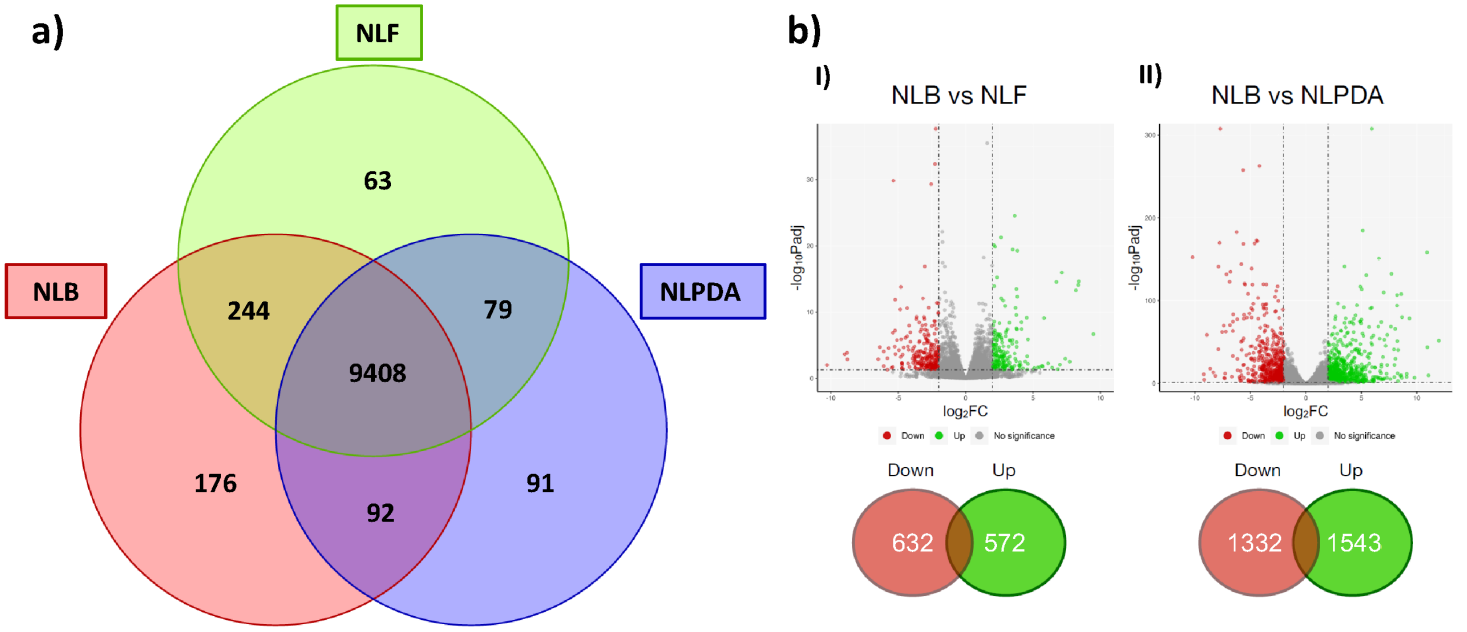


Figure 6

Differential gene expression analysis in *N. luteum*. (**a**) Venn diagram showing transcript overlap between growth conditions. Numbers of common and specific transcripts obtained in the transcriptome analysis of *N. luteum* growing on avocado branches (NLB), *N. luteum* growing on avocado fruits (NLF) and *N. luteum* growing on PDA (NLPDA). Unique transcripts are shown in only one of the circles while shared transcripts are illustrated where the circles meet. (**b**) Volcano plots of differentially expressed genes (DEGs) for pairwise comparisons: (I) NLB vs. NLF and (II) NLB vs. NLPDA. Green and red dots represent significantly upregulated and downregulated genes (−2 > fold change (FC) > 2; $P < 0.05$), respectively; grey dots indicate non-significant changes.

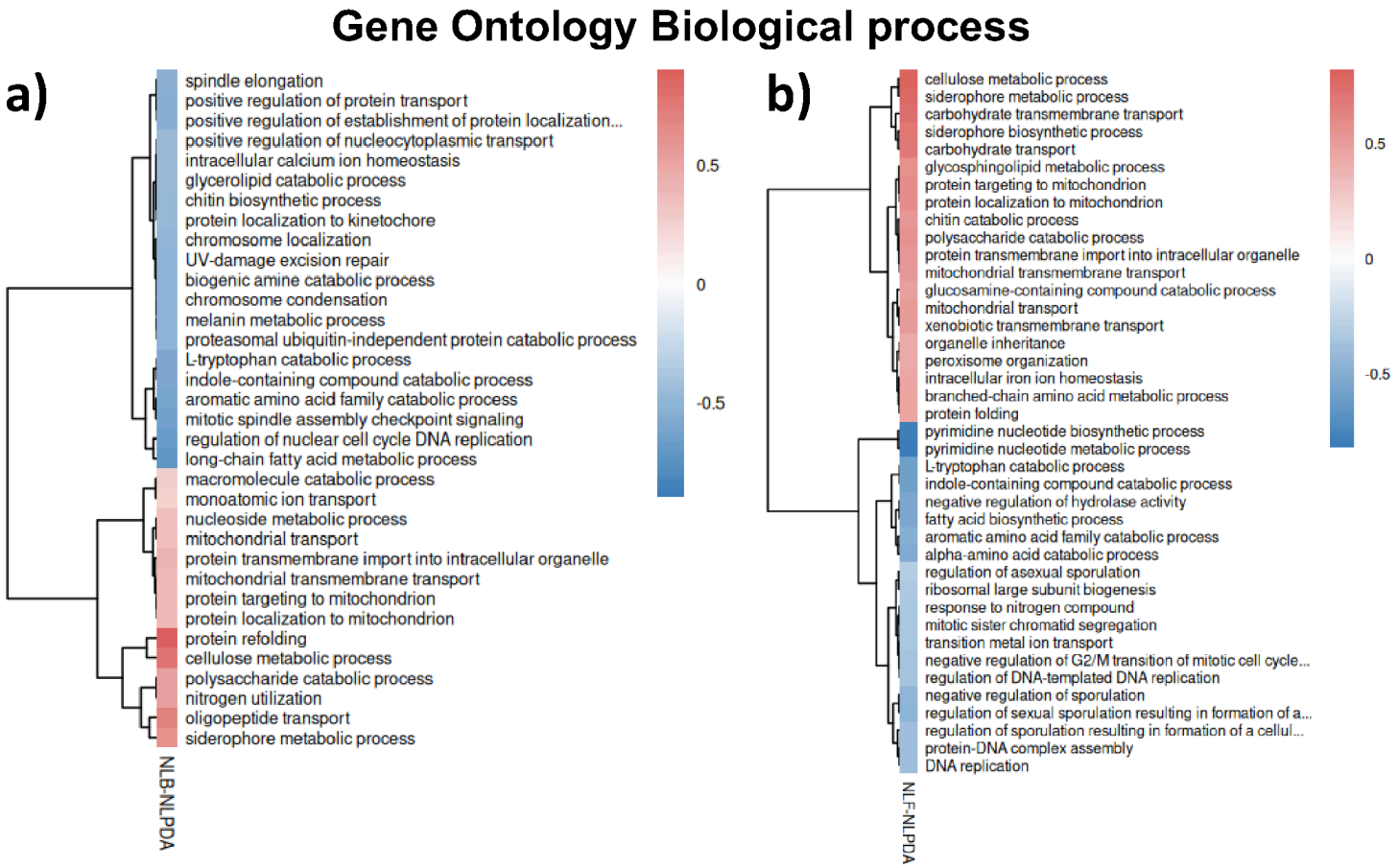


Figure 7

Gene ontology (GO) enrichment analysis of differentially expressed genes (DEGs). GO Biological process (BP) enrichment of *N luteum* DEGs from infected avocado branches (A) and fruits (B) in comparison with Potato Dextrose Agar media (PDA). P-value threshold < 0.05.

Supplementary Files

This is a list of supplementary files associated with this preprint. Click to download.

- Suplementarytable1.docx